

General linear correction method for DFT+ X energy: application to U-M (M=Al, Ga, In) alloys under high pressure

Xiao L. Pan^{1,2,3}, Hong X. Song¹, Y. Sun¹, F. C. Wu^{1*}, H. Wang¹, Y. F. Wang¹, Y. Chen⁵, Xiang R. Chen^{2*}, Hua Y. Geng^{1,4*}

¹ National Key Laboratory of Shock Wave and Detonation Physics, Institute of Fluid Physics, China Academy of Engineering Physics, Mianyang, Sichuan 621900, P. R. China;

² College of Physics, Sichuan University, Chengdu 610065, P. R. China;

³ Extreme Condition Material Properties Science and Technology center, School of Mathematics and Physics, Southwest University of Science and Technology, Mianyang, 621010, P. R. China;

⁴ HEDPS, Center for Applied Physics and Technology, and College of Engineering, Peking University, Beijing 100871, P. R. China;

⁵ Fracture and Reliability Research Institute, School of Engineering, Tohoku University, Sendai 980-8579, Japan.

Abstract: DFT+ X methods, such as DFT+ U and DFT+DMFT, are important supplements to standard density functional theory when strong on-site Coulomb interactions are present. However, the involvement of external parameters in the underlying model Hamiltonian introduces intrinsic ambiguity when comparing the total energies obtained with different model parameters. This renders DFT+ X approaches semi-empirical and severely hinders their capability to describe phase ordering and phase stability, especially when reliable experimental benchmarks are unavailable, such as under high pressure. In this work, we resolve this longstanding problem by proposing a general linear correction method that eliminates the ambiguous energy contributions introduced by the model Hamiltonian in DFT+ X approaches, thereby enabling direct comparison of their energies calculated with different interaction parameters. The method is demonstrated and validated within the framework of DFT+ U , an important member of the DFT+ X family. It is then applied to important nuclear materials of uranium-based binaries U-M (M=Al, Ga, In) alloys. With this approach, we resolve the long-standing discrepancy between theoretical predictions and experimental observations of phase stability with unprecedented accuracy, and predict several

* Corresponding authors. E-mail: s102genghy@caep.cn; xrchen@scu.edu.cn; fcwu2011@mail.ustc.edu.cn

previously unknown stable intermetallic compounds under high pressure. The broad applicability of the method is further confirmed by accurate predictions of formation enthalpies for diverse systems, including Np-Al, U-Si, and Cu-O binaries, the ternary MnSnAu compound, and oxygen adsorption on the Cu(111) surface. This work establishes linear-corrected DFT+ U as a fully first-principles approach and validates the linear correction method as a robust and general scheme that can be readily extended to other DFT+ X methods.

Keywords: strong correlation; on-site Coulomb interaction; DFT+ X method; phase stability; high pressure

I. Introduction

Due to its good balance between high efficiency and accuracy, density functional theory (DFT) [1, 2] has grown into a workhorse of condensed matter physics and materials science [3-6], where phase stability/ordering and phase diagrams are usually among the most important physical properties that are widely investigated. Regardless of its initial success in simple metals, DFT suffers from the self-interaction error (SIE) [7] and provides an inaccurate description of strong electronic correlations when orbitals become localized, a deficiency intrinsic to all static mean-field theories. This causes the commonly used local and semi-local exchange–correlation functionals, such as the local density approximation (LDA) [2], the generalized gradient approximation (GGA) [8], and even the most advanced SCAN functional [9], to underestimate band gaps in semiconductors and insulators [10, 11]. The total energies of strongly correlated systems with localized d or f electrons are also poorly described [12, 13]. Hybrid functionals, which incorporate a fraction of exact exchange, can partially alleviate this problem; however, they significantly increase the computational cost and may introduce additional issues such as localization errors [14].

In contrast, combining DFT with the phenomenological Hubbard model for localized orbitals shows great promise in addressing these problems. This line of strategy has produced a family of methods collectively referred to as DFT+ X , including DFT+ U [11, 15], DFT+ G [16, 17], DFT+DMFT [18, 19], and DFT+ J [14]. For all of these methods, the model Hamiltonian depends on the empirical Hubbard parameters U and J (or the effective U - J), which describe the strength of on-site Coulomb interactions. The total energy of DFT+ X is thus a function of these external parameters, which are unfortunately not well-defined and contain ambiguity. The most notorious consequence is that energies calculated with different values of these parameters cannot be directly compared. Even worse, these parameters usually vary with pressure [12], chemical compositions, and even local atomic environment [20], making the determination of phase stability and phase diagrams using DFT+ X methods highly problematic, if not impossible. To address this issue, several methods that rely on

experimental information have been proposed in recent years [21, 22, 23, 24], primarily focusing on the DFT+ U formalism because of its simplicity and high computational efficiency. The extension of these methods to other DFT+ X approaches is straightforward.

It should also be mentioned that some DFT+ U calculations in the literature directly compare uncorrected DFT+ U total energies obtained with different values of U . Such a practice, however, is very risky and should be adopted only when reliable experimental or theoretical data, such as cohesive energy or formation energy [21], are available and can be used as the reference. Similarly, for reactions in which only some reactants possess localized orbitals, calculating the reaction enthalpy requires comparing and mixing the energy obtained from DFT and DFT+ U . In this situation, the plain approach mentioned above is clearly not applicable. To this end, Jain et al. proposed a mixed GGA/GGA+ U scheme [22] in which the DFT+ U energies are recalibrated with respect to available experimental data. Specifically, the GGA+ U energies are *adjusted* to align with the averaged experimental trends. This tentatively achieves the compatibility between the calculated DFT+ U and DFT energies, and yielding acceptable formation enthalpies. Another closely related method, the fitted elemental-phase reference energies (FERE) method [23, 24], uses the experimental formation enthalpies of selected compounds together with their DFT+ U total energies to derive the *artificial* elemental reference phase energies by solving a linear least-squares problem. These reference energies are then employed to compute the formation enthalpies of other compounds that are chemically and physically similar. Using this method, accurate formation enthalpies have been obtained for transition metal binary oxides [25] and metal sulfides [26], as intended.

Nevertheless, all of these methods rely entirely on experimental formation enthalpies to correct DFT+ U energies, rendering the latter essentially empirical. Unfortunately, accurate experimental data are scarce and often unavailable for most newly discovered materials. The same is true for common materials under extreme conditions, such as high pressure. Therefore, these methods (and their variants) cannot be applied in situations where no experimental data are available. In this context,

accelerating materials design and discovery calls for a novel theoretical framework capable of correcting DFT+ X energies without relying on experimental data.

In this work, we propose a general correction method for DFT+ X energies (and enthalpies) that does not require any experimental or other theoretical reference data. The implementation of the method within the DFT+ U framework is illustrated. The method is validated for U-Ga and U-Al systems at ambient conditions by comparison with available experimental data. It is then applied to U-M (M = Al, Ga, In) systems under high pressure, all of which are important nuclear materials. Several previously unknown phases have been predicted, which would have been inaccessible without the consistent theoretical framework provided by this correction method for accurately calculating formation enthalpies of strongly correlated systems using DFT+ X under extreme conditions. Furthermore, the broad applicability of the method is demonstrated through successful applications to other complex systems, including binary systems such as U-Si, Np-Al, and Cu-O, as well as the adsorption formation enthalpy of oxygen on the Cu(111) surface and the formation enthalpy of the ternary MnSnAu compound.

II. Theoretical formalism

A. General consideration

It is evident that the goal of all the aforementioned corrections to the DFT+ U energies is to render them compatible with pure DFT, such that the resulting energies can be directly compared. Previously, this is done by removing the ambiguity in DFT+ U energy by directly using experimental formation enthalpies in the mixed GGA/GGA+ U method [22], or by introducing artificial elemental reference energies with the aid of experimental data in the FERE method [24]. Nevertheless, we should point out that it is theoretically possible to remove such ambiguity without resorting to any experimental guidance. This fully *ab initio* capability is highly desirable, particularly given the rapidly expanding classes of novel materials and their applications under extreme conditions, where reliable energy information is essential but experimental data are often unavailable. Unfortunately, no such approach has been reported in the literature to date.

Such a correction may be formulated at the level of local atomic approximation, namely by assuming that the unphysical contribution responsible for the ambiguity is confined within individual atoms. We are reminded of the cohesive energy definition of condensed matter, which ensures compatibility among different exchange–correlation (XC) functionals in DFT. Following similar idea, a “cohesive energy” can be defined within the DFT+ U framework by subtracting the atomic energy—calculated using DFT+ U with the same value of the Hubbard parameters—from the total energy. A practical difficulty of this approach is that, when performing DFT+ U calculations for isolated atoms, most currently available DFT codes encounter severe numerical convergence problems. This technical limitation prevents the application of such a naive local atomic correction.

On the other hand, we note that in all DFT+ X methods the introduced Hubbard model Hamiltonian contains terms that depend linearly on the model parameters such as U and/or J . These extrinsic terms have two physical effects: (i) they tune the electronic density to a more appropriate distribution, (ii) they contribute to the energy directly. According to the Hohenberg-Kohn theorem [1], the ground-state electronic density uniquely determines the entire electronic system. Therefore, if a DFT+ X method properly describes a system, it should produce an accurate density, and this density must be close to that of the exact DFT. Although there is no exact XC functional for DFT available yet, advanced functionals such as SCAN [9] can be employed to evaluate accurate energies from a given DFT+ X density. Following this reasoning, we can combine the DFT+ U density with the SCAN functional to remove the ambiguity in the former and make it compatible with the pure DFT. The theoretical basis of this approach is that the main error in DFT is the density-driven error and functional-driven error; and for a given density and a sufficiently accurate functional such as SCAN, the functional-driven error should be minor. In practice, one could first perform a DFT+ U calculation to obtain the electronic density, which is then fed into the pure DFT with SCAN functional to acquire the energy while keeping the density unchanged. This non-self-consistent scheme, which combines the DFT+ U density with the SCAN functional, is inspired by previous work aimed at correcting density-driven errors in pure DFT such

as Ref. [27], and is conceptually similar in nature. Unfortunately, in practice we found that this approach is applicable only at ambient conditions, where pressure or stress effects are negligible. Otherwise, this non-self-consistent approach usually gives a quite different pressure or stress from that of DFT+ U , making it very difficult to align the enthalpy to the given pressure/stress, which is essential for calculating the phase stability and phase diagrams at elevated pressures.

B. Linear correction method (LCM)

Based on the general considerations as mentioned above, we introduce a linear correction method (LCM) to address this issue. Taking the simplified approach to DFT+ U proposed by Dudarev *et al.* [11] as an example, the introduced Hubbard model Hamiltonian can be reduced to an energy functional supplemented to the pure DFT as:

$$E_{\text{DFT}+U} = E_{\text{DFT}} + \frac{U}{2} \sum_{\sigma} (n_{m,\sigma} - n_{m,\sigma}^2), \quad (1)$$

where U is the effective Hubbard parameter, $n_{m,\sigma}$ is the occupation number of the m -th state with a spin of σ . The resulting total energy expressed in terms of the Kohn-Sham eigenvalues is

$$E_{\text{DFT}+U} = E_{\text{DFT}}[\{\varepsilon_i\}] + \frac{U}{2} \sum_{l,j,\sigma} \rho_{lj}^{\sigma} \rho_{jl}^{\sigma}, \quad (2)$$

in which the second term represents the double-counting correction, and ρ_{lj}^{σ} is the density matrix [11]. It is evident that the energy is a function of U and a functional of density, *i.e.*, $E = E(U, [n])$. In contrast, what is expected from DFT is purely $E = E([n])$ [1, 2]. The explicit dependence of the energy on U is unphysical and should be removed in order to obtain an unambiguous energy that can be directly compared with pure DFT results or experimental data. As can be seen from Eqs. (1) and (2), this dependence is

linear with respect to U . Motivated by this observation, a linear correction method (LCM) for DFT+ U energy can be proposed as

$$E_{\text{DFT}+U}^{\text{LC}} = E_{\text{DFT}+U} - \left(\frac{\partial E}{\partial U} \right)_{[n_{\text{loc}}]} U. \quad (3)$$

Here, the superscript LC indicates the quantity already corrected by LCM, and the subscript n_{loc} in the second term indicates that the partial derivative is performed under the constraint that the localized charge density around the target atoms remains unchanged (Namely, in the sense of *local atomic approximation*). In practice, we can assume that for given systems that are chemically similar, the derivative in Eq. (3) can be approximated as a constant. As a result, the LCM corrected total energy per unit cell is given by

$$E_{\text{DFT}+U}^{\text{LC}} = E_{\text{DFT}+U} - \epsilon \sum_{i=1}^N U_i \quad (4)$$

where ϵ is a constant, U_i is the value of parameter U for i -th atom, and N is the total number of atoms in the unit cell. All quantities in Eq. (4) can be obtained directly from first-principles calculations.

To illustrate how the LCM can be applied to DFT+ X , we consider a binary system as an example. Specifically, for a binary system A_xB_y , the formation enthalpy is defined as:

$$\Delta H_{A_xB_y}^f = (H_{A_xB_y} - xH_A - yH_B) / (x + y) \quad (5)$$

where $H_{A_xB_y}$ is the enthalpy per formula unit of the compound A_xB_y , and H_A and H_B represent the enthalpy per atom of elements A and B, respectively. At a given pressure, the enthalpy is given by $H=E+PV$, where V represents the specific volume.

We assume that the localized orbitals of atom A are strongly correlated and therefore require special treatment within a DFT+ X framework (represented here by DFT+ U for simplicity), whereas atom B is weakly correlated and can be well described by pure DFT. We further note that the correction to PV term is typically small. Therefore, the LCM is applied only to the internal energy E . This argument is justified because pressure is given by the first derivative of the energy with respect to volume. Within the framework of DFT+ U , it can be expressed as

$$P = -\frac{\partial E([n], U)}{\partial V} = -\frac{\partial E}{\partial n} \Big|_U \frac{\partial n}{\partial V} - \frac{\partial E}{\partial U} \Big|_{[n]} \frac{\partial U}{\partial V}. \quad (6)$$

The variation of localized part $\frac{\partial E}{\partial U} \Big|_{[n_{\text{loc}}]}$ is unphysical, and must be removed. We thus have

$$P_{\text{DFT+U}}^{\text{LC}} = P_{\text{DFT+U}} + \epsilon \frac{\partial U}{\partial V}. \quad (7)$$

The second term in Eq. (7) is the contribution that requires LCM correction when evaluating the pressure. In general, the value of U remains nearly constant over a small range of density variations, so that $\frac{\partial U}{\partial V} \approx 0$. However, for sufficiently large volume changes, the slope $\frac{\partial U}{\partial V}$ may become finite, and the pressure should then be corrected accordingly. However, if the magnitude of this correction is small, when we realign the enthalpy to the given pressure, the correction to enthalpy from the PV term is cancelled by the leading correction from the internal energy, leaving only higher-order corrections that can be safely neglected [28]. Therefore, in any case, the correction to enthalpy can be approximated by the correction to the internal energy.

To apply LCM, we first notice from Eq. (4), that the energy difference between two chemically similar but compositionally different compounds (e.g., A_xB_y and $A_x'B_{y'}$),

after properly subtracting the contributions of the B atoms, is proportional to the constant ϵ . That is,

$$\Delta E = (y'E_{A_xB_y}^{\text{DFT}+U} - y'E_{A_xB_{y'}}^{\text{DFT}+U}) - (y'E_{A_xB_y}^{\text{DFT}} - y'E_{A_xB_{y'}}^{\text{DFT}}) = \Delta N_U \cdot \epsilon \quad (8)$$

where ϵ is the constant defined in Eq. (4), and ΔN_U is defined as the difference in the effective Hubbard U strength between the two compounds in the DFT+ U calculations, which is given by

$$\Delta N_U = y'N_U(A_xB_y) - yN_U(A_xB_{y'}), \quad (9)$$

with

$$N_U(A_xB_y) = \sum_{i=1}^{N_A} U_i, \quad (10)$$

where N_A is the total number of A-type atoms, and U_i is the Hubbard U value for the i -th A atom. For example, for compound U_2Al_3 in which each uranium atom has been described by DFT+ U with an effective Hubbard value of $U=2.5$ eV, then its N_U can be calculated as $N_U(U_2Al_3) = \sum_{i=1}^2 U_i = 2.5 + 2.5 = 5$ eV.

For any given pair of compounds, once the U values have been specified for each atom, the ΔN_U can be determined by Eq. (9), which then can be subsequently substituted into Eq. (8). On the other hand, the energy difference ΔE defined in Eq. (8) (*i.e.*, the first equality in Eq.(8)) can be obtained directly from the corresponding DFT+ U and DFT total energy calculations. The two quantities therefore can form a data pair $(\Delta E, \Delta N_U)$. This procedure can be repeated for all possible pairs of compounds, yielding a set of $(\Delta E, \Delta N_U)$ data points. The total number of such data pairs is C_M^2 , where M is the number of distinct compounds considered. For example, if we consider 10 different compositions of A_xB_y compounds, a total of $C_{10}^2 = 45$ data

points of $(\Delta E, \Delta N_U)$ pair can be obtained. This data set can be used to assess the validity of the linear relationship as assumed in the second equality of Eq. (8). Moreover, it can be employed to determine the constant ϵ in Eq. (8) through linear fitting.

It is necessary to point out that if ϵ is not a constant, Eq. (8) cannot be held any more, and we need go back to Eq. (3). In any case, ϵ always can be expressed as a function of U , i.e., $\epsilon = \epsilon(U)$. Therefore, Eq. (3) should be replaced by

$$E_{\text{DFT}+U}^{\text{LC}} = E_{\text{DFT}+U} - \int_0^U \epsilon(U') \cdot dU', \quad (11)$$

in which $\epsilon(U') = \frac{\partial E}{\partial U} |_{[n_{\text{loc}}], U=U'}$ and can be determined by the slope of $E([n], U)$ with respect to U at the condition that the localized charge density n_{loc} is fixed, then the LCM is still applicable. As will be seen, in all cases we explored here, the linearity relation holds very well, and $\int_0^U \epsilon(U') dU'$ reduces to $\epsilon \cdot U$, which then gives Eq. (8).

Once Eq. (8) is validated and the value of ϵ constant is determined, the DFT+ U internal energy for each binary compound of $A_x B_y$ can be reliably corrected by

$$E_{\text{DFT}+U}^{\text{LC}} = E_{\text{DFT}+U} - \Delta_U, \quad (12)$$

where $\Delta_U = \epsilon \cdot \sum_{i=1}^{N_A} U_i$. Similarly, the enthalpy is corrected by $H_{\text{DFT}+U}^{\text{LC}} = H_{\text{DFT}+U} - \Delta_U$.

The formation enthalpy defined in Eq. (5) is then corrected by LCM as:

$$\Delta H_{A_x B_y}^{f, \text{LC}} = \frac{(H_{A_x B_y}^{\text{DFT}+U} - \Delta_U) - (xH_A^{\text{DFT}} + yH_B^{\text{DFT}})}{x+y}, \quad (13)$$

which can now be directly compared with experimental data and subsequently used to determine the phase stability and phase diagram of the system (here we have assumed that the elemental phase A and B do not require DFT+ U treatment).

Although DFT+ U is employed here as an illustrative example to demonstrate the

LCM, the method itself does not depend on the specific theoretical details of how the Hubbard model is implemented. The same reasoning that leads to Eqs. (4, 7, 8, 12, 13) can be readily extended to other DFT+ X approaches. Such generalizations are straightforward and will not be elaborated here. It should also be pointed out that the LCM can be applied to multi-component systems containing two or more distinct strongly correlated species. The only thing that one should be cautioned is that each species could have its own constant ϵ in that situation.

III. Validation and application

A. Validation of LCM

We validate the LCM from two complementary aspects: First, we demonstrate that the linear relationship assumed in Eq. (8) holds in practice. Second, we compare the formation enthalpies obtained from Eq. (13) with available experimental data to show that accurate formation enthalpies can be achieved within DFT+ U without using any experimental information as input. For this purpose, we take Uranium-Gallium (U-Ga) system as a representative example. First-principles structure prediction methods are employed to identify the most stable candidate structures at zero pressure for ten possible stoichiometries of U_xGa_y compounds (with $x:y = 4:1, 3:1, 2:1, 3:2, 1:1, 2:3, 3:5, 1:2, 1:3, 1:4$). For these ten distinct compounds, there are $C_{10}^2 = 45$ unique compound pairs. Using Eqs. (8) and (9), we obtain 45 respective data points in the form of $(\Delta E, \Delta N_U)$. The specific U values adopted for uranium atoms in each compound are provided in Fig. S1 of the Supplementary Material (SM). These data are plotted in Fig. 1(a). As shown in Fig. 1(a), the data exhibit an excellent linear relationship, thereby

validating the linearity assumption of Eq. (8). By performing a least-squares fit of Eq. (8) to the 45 first-principles data points, the dimensionless constant ϵ for the U-Ga system under ambient conditions is determined to be $\epsilon=1.1122$.

To assess the accuracy of LCM, we calculate the formation enthalpies using Eq. (13) with this ϵ value. The resulting convex hull constructed from the LCM-corrected formation enthalpies is shown by the red lines in Fig. 1(b), together with the pure DFT convex hull and the experimental data for U-Ga system [29, 30] for comparison. Note that these experimental data were measured at room temperature where the U_xGa_y compounds are in non-magnetic (NM) state. To ensure a consistent comparison, all compounds are treated as NM in both the DFT+ U and pure DFT calculations. The uncorrected convex hull obtained directly from DFT+ U is provided in Fig. S2 of the SM. We find that the convex hull predicted by plain DFT+ U is unphysical: the formation enthalpies deviate significantly from the experimental data, and no stable compounds are predicted. Pure DFT performs better in this regard, with the shape of its convex hull qualitatively similar to the experimental one. However, the formation enthalpy of UGa_3 is overestimated by approximately 63.7% compared with the averaged experimental value. Moreover, pure DFT fails to predict the stability of UGa_2 and incorrectly yields two stable compounds, U_2Ga and U_2Ga_3 , indicating that pure DFT is insufficient to accurately describe the U–Ga system. In contrast, the LCM-corrected DFT+ U results yield an accurate convex hull for the U-Ga system and correctly predict the stability of UGa_2 and U_2Ga_3 at zero pressure. Notably, the predicted formation enthalpies are well bracketed by the experimental data: the

predicted $\Delta H_{\text{UGa}_3}^{f,\text{LCM}}$ is just about 5.2% away from the calorimetry data, while that of UGa_2 is only 4.6% away from the average of the experimental data (about 10 folds better than pure DFT). Furthermore, the predicted crystal structures of UGa_2 (space group $P6/mmm$) and UGa_3 (space group $Pm-3m$) are in excellent agreement with experimental observations.

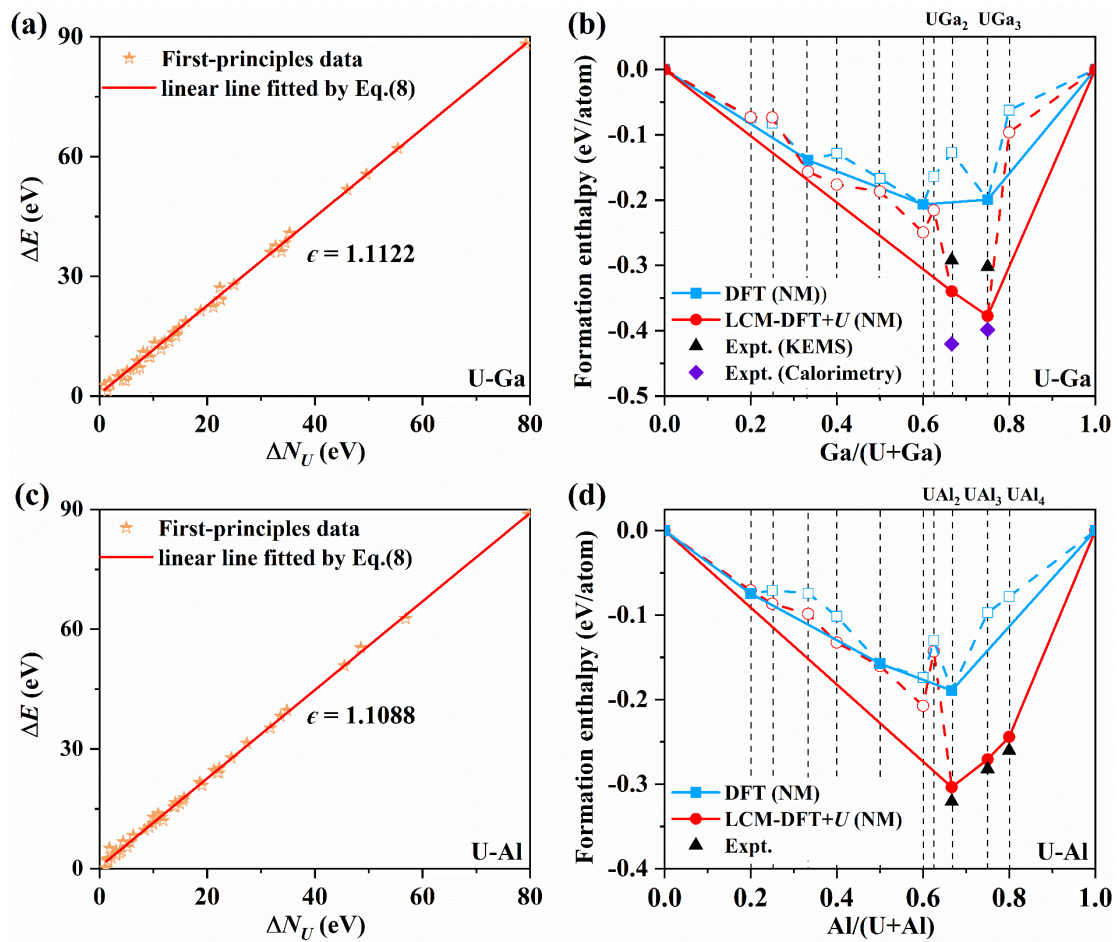


Fig. 1 (color online) Calculated ΔE - ΔN_U points and the corresponding linear fits obtained using Eq. (8) at ambient conditions for (a) U-Ga and (c) U-Al systems. Thermodynamic convex hulls of candidate structures at ambient conditions calculated using pure DFT and DFT+ U with LCM method are shown for (b) the U-Ga system and (d) the U-Al system. Experimental data for the U-Ga system are taken from Knudsen

effusion mass spectrometry (KEMS) [29] and Calorimetry measurements [30], while experimental data for the U-Al system are taken from Ref. [31]. Dashed lines indicate unstable or metastable phases, whereas solid lines denote thermodynamically stable phases.

To further corroborate the validity of the LCM, we examine another system, the U-Al alloys, under ambient conditions. Ten representative stoichiometries are considered, yielding ten distinct candidate compounds. Pairwise combination of these compounds results in a total of $C_{10}^2 = 45$ data tuples $(\Delta E, \Delta N_U)$ as defined by Eq. (8). These data are plotted in Fig. 1(c). As expected, the data exhibit a clear linear relationship. The corresponding constant ϵ is determined to be $\epsilon=1.1088$, which is very close to the value obtained for the U-Ga system. In fact, the linearity between $(\Delta E, \Delta N_U)$, as stated in Eq. (8), is not sensitive to the specific chemical system or pressure. Instead, it represents a general feature of the LCM, as further demonstrated for additional systems in Figs. S4–S6 of the SM.

The formation enthalpies and the corresponding convex hull obtained from the LCM are compared with those from pure DFT and available experimental data in Fig. 1(d) [31]. The comparison with plain DFT+ U is also illustrated in Fig. S2 of the SM. It is evident that neither plain DFT+ U nor pure DFT provides an adequate description of the U–Al system. Especially, plain DFT+ U fails to predict any stable U_xAl_y compounds. Pure DFT fails to predict the stability of UAl_3 and UAl_4 at zero pressure, and falsely predicts that U_2Al and UAl are stable. Even for UAl_2 , the pure DFT predicted enthalpy

is about 65.6% higher than the experimental data. In contrast, the LCM of DFT+ U method correctly predicts the stability of UAl_2 , UAl_3 , and UAl_4 on the convex hull, which is in good agreement with the experimental observation. The predicted crystal structures of MgNi₂-type $P6_3/mmc$ - UAl_2 , $Pm-3m$ - UAl_3 and $Imma$ - UAl_4 are consistent with those reported in previous experimental studies [32-35]. Most importantly, the LCM-corrected formation enthalpies show excellent quantitative agreement with the experiments, with deviations of only 5.3% for UAl_2 , and 4.1% and 6.2% for UAl_3 and UAl_4 , respectively.

B. Discovery of new high-pressure phases of U-M (M= Ga, Al, In) alloys by LCM

As mentioned above, the LCM applied to DFT+ U not only reproduces the correct phase stability and phase diagrams of the U-Ga and U-Al systems at ambient conditions, but also yields quantitatively accurate formation enthalpies. To the best of our knowledge, this is the first time that their phase stability and formation enthalpy are correctly predicted from pure first-principles, without any experimental input. Using this method, we further identified that the previously proposed $Cmcm$ - U_3Ga_5 and MgCu₂-type $Pd-3m$ - UAl_2 phases reported in earlier studies [33, 36, 37] are in fact metastable and not thermodynamically stable at zero pressure. As pointed out in Sec. II, LCM does not rely on pressure or other external conditions. Its demonstrative accuracy at zero pressure, together with the crucial advantage that no experimental data are required as input, enables reliable investigation of strongly correlated materials under extreme conditions, such as high pressure, where experimental energetic data are

scarce or entirely unavailable. In this subsection, we focus on the important nuclear materials of U-M (M=Ga, Al, In) alloys. By combining first-principles structure predictions together with the LCM-corrected DFT+ U approach, we explore the most stable structures of U_xGa_y compounds at pressures of 25, 50, 100, 150 and 200 GPa, respectively. The linearity of $(\Delta E, \Delta N_U)$ tuple for all of these candidate structures of U_xGa_y are checked for each pressure separately; and the constant ϵ for each pressure is obtained by least square fitting to Eq. (8) (Fig. S4).

The convex hull diagram of U-Ga system at 0 K, constructed using the formation enthalpies calculated with the LCM-corrected DFT+ U method, is shown in Fig. 2(a). Note that, here the proper magnetic ordering (FM, AFM, or NM) has been taken into account in all DFT+ U calculations, which is different from Fig. 1 where the temperature is room temperature and the magnetic state is NM. At zero pressure, the difference in magnetic ordering leads to a little deeper formation enthalpy, but does not affect the stability of competing structures. Figure 2(b) demonstrates the 0 K phase diagram of U-Ga system, in which the pressure ranges of the stable phases are shown. As can be seen, only the AlB₂-type $P6/mmm$ -UGa₂ and Cu₃Au-type $Pm-3m$ -UGa₃ phases are stable at zero pressure, which is in line with previous experimental studies [38, 39]. Upon increasing pressure, $P6/mmm$ -UGa₂ phase becomes unstable at a pressure of 13 GPa, whereas the $Pm-3m$ -UGa₃ phase transforms into a hexagonal $P6/mmm$ phase at 44.7 GPa, which remains stable up to 82 GPa. For other Ga-rich compositions, we predict a previously unknown U₂Ga₃ compound that is stable between 45–200 GPa. It adopts a hexagonal structure with space group $P-62m$. On the U-rich side, a new U₂Ga

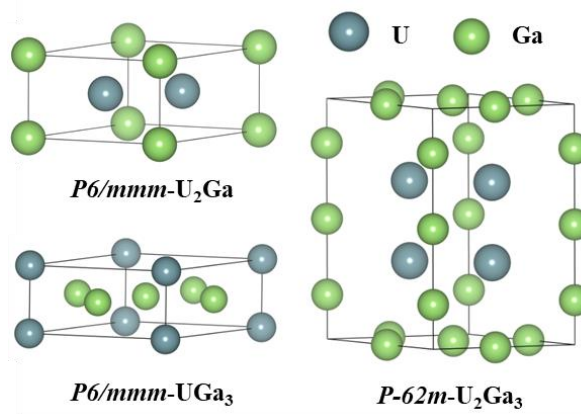


Fig. 3 (color online) Structure of the newly predicted stable intermetallic compounds in U-Ga system.

Furthermore, the lattice parameters and magnetic moments of the UGa_2 and UGa_3 compounds calculated using DFT+ U at 0 GPa and 0 K are compared with available low-temperature experimental data. Good agreement is obtained between theory and experiment. By contrast, pure DFT significantly underestimates the magnetic moments, as shown in Table 1. In addition, our study reveals that the previously proposed but controversial Pu_3Pd_5 -type $Cmcm-U_3Ga_5$ phase is in fact not thermodynamically stable. It is quite close to the convex hull at zero pressure (with a distance of 0.12 eV/atom), and should be regarded as metastable. The calculated lattice parameters and magnetic moment of this U_3Ga_5 compound are also consistent with the reported experimental data (Table 1).

Table 1. Calculated lattice parameters and orbital (μ_L) and spin (μ_S) magnetic moment per uranium atom for $P6/mmm-UGa_2$, $Pm-3m-UGa_3$ and $Cmcm-U_3Ga_5$ phases at zero pressure, along with previous theoretical and experimental data, respectively.

Phase	Method	Lattice parameters	Axis	Magnetic order	u_L (μ_B)	u_S (μ_B)	$ u_L+u_S $ (μ_B)
UGa ₂	PBE	a=b=4.230 c=3.990	100	FM	-2.953	2.23	0.72
	PBE+ <i>U</i>	a=b=4.248 c=4.075	100	FM	-3.662	1.553	2.11
	Expt. [42]	a=b=4.213 c=4.020	100	FM	—	—	2.70
UGa ₃	PBE	a=b=c=4.265	111	AFM	-1.797	2.203	0.41
	PBE+ <i>U</i>	a=b=c=4.316	111	AFM	-2.914	2.274	0.64
	LDA+ <i>U</i> [43]	—	111	AFM	-3.02	2.38	0.64
	Expt. [44]	a=b=c=4.240	111	AFM	—	—	0.74
U ₃ Ga ₅	PBE+ <i>U</i>	a=9.502 b=7.789 c= 9.505	001	FM	-0.953	2.235	1.28
	Expt. [37, 38]	a=9.442 b=7.629 c=9.449	001	FM	—	—	1.1

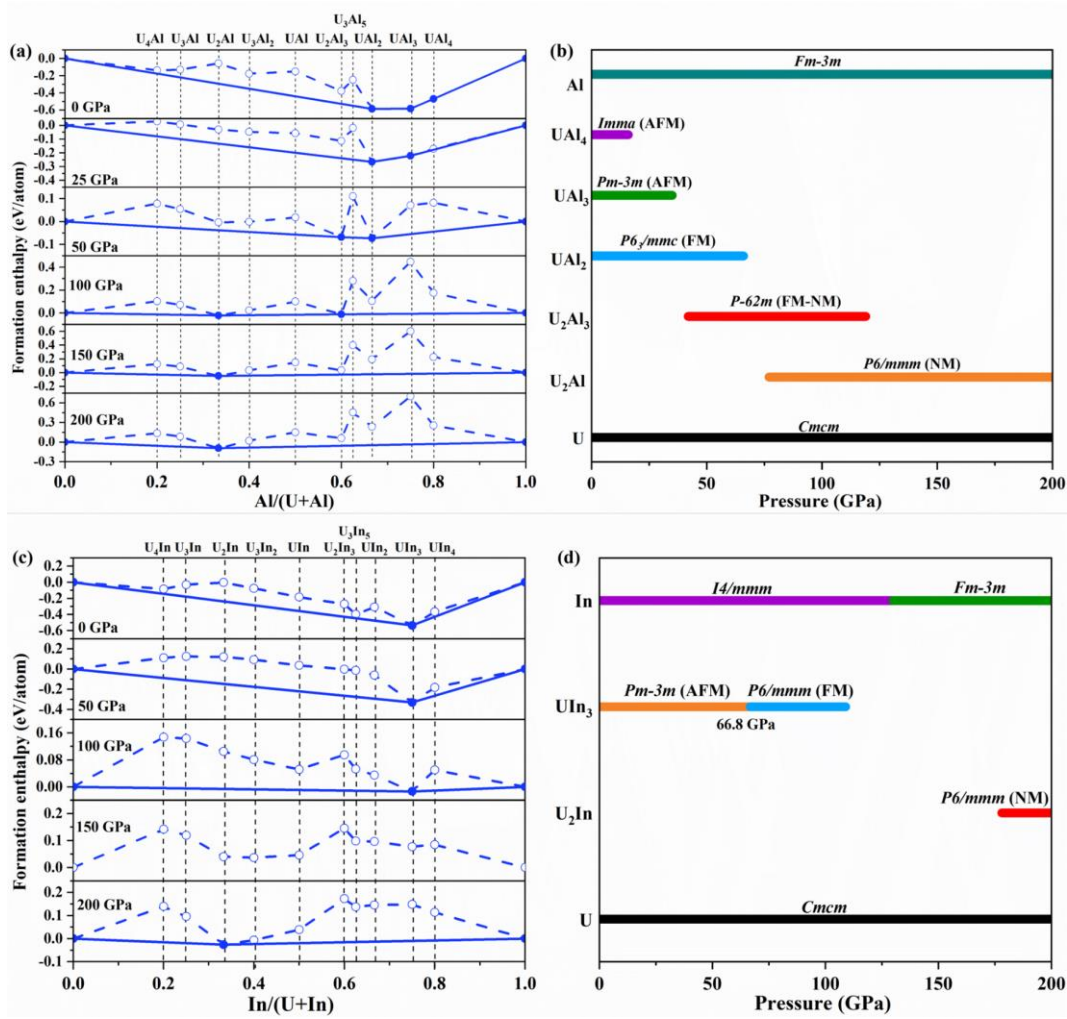


Fig. 4 (color online) Thermodynamic convex hull diagrams of candidate structures for (a) U-Al and (c) U-In systems at different pressures and 0 K calculated with LCM for DFT+ U method. The corresponding composition-pressure phase diagrams at 0 K for (b) U-Al and (d) U-In systems, in the range of 0–200 GPa, respectively.

We further apply the LCM to U-Al and U-In systems at high pressures up to 200 GPa. The calculated thermodynamic convex hull and composition-pressure phase diagrams of U-Al and U-In alloys at 0 K are shown in Fig. 4. At low temperature, all of these structures exhibit nontrivial magnetic orderings. At zero pressure, we find that UA₂, UA₃, and UA₄ still remain thermodynamically stable at 0 K, but their magnetic

orderings change from NM at room temperature to FM or AFM at 0 K. With increasing pressure, the $P6_3/mmc$ -UAl₂, $Pm-3m$ -UAl₃, and $Imma$ -UAl₄ phases lose stability at 66, 35, and 16 GPa, respectively. In contrast, new compounds with different stoichiometries, namely $P6/mmm$ -U₂Al and $P-62m$ -U₂Al₃, become stable in the pressure ranges of 77–200 GPa and 42–119 GPa, respectively.

Unlike the U-Al and U-Ga alloys, only one thermodynamically stable phase, $Pm-3m$ -UIn₃, is found for the U-In system at zero pressure (Fig. 4(c, d)), in agreement with experimental observation [45]. With increasing pressure, this structure transforms into a hexagonal $P6/mmm$ phase at 66.8 GPa, which remains stable up to 130 GPa. Notably, a similar structural transition is also predicted for UGa₃ (Fig. 2). At higher pressures, only one compound with the stoichiometry U₂In and space group of $P6/mmm$ is found to be stable, with a stability range of 178–200 GPa.

It is worth noting that although UIn₃ exhibits AFM ordering at low temperature, it becomes paramagnetic (PM) at room temperature. For this reason, we also examine the phase stability of the NM or PM states of U_xIn_y compounds under ambient conditions. The corresponding (ΔE , ΔN_U) data tuple and the formation enthalpy calculated using the LCM of DFT+ U are obtained. Comparisons with the plain DFT+ U , pure DFT and experimental data are presented in Fig. S3. Once again, the LCM-DFT+ U accurately reproduces the experimental formation enthalpy of the UIn₃ compound. In contrast, both pure DFT and plain DFT+ U incorrectly predict that no stable intermetallic compounds exist in the U-In system. This result further confirms the effectiveness and robustness of the LCM.

IV. Discussion

In the preceding section, we applied the LCM to U-based binary alloys and demonstrated its effectiveness. In order to verify the broader applicability of LCM, we further explore other binary compounds beyond uranium alloys, as well as more complex ternary compound and surface adsorption problem. In the first case, we applied the LCM-DFT+ U method to the Np-Al and U-Si systems, with the results shown in Fig. 5. For the Np-Al system, the formation enthalpies predicted by pure DFT deviate substantially from the reference values obtained from CALPHAD assessments [46], showing an average error of 67.8%; and the NpAl_3 compound is wrongly predicted as unstable. In contrast, the LCM method correctly predicts the phase stability of NpAl_2 , NpAl_3 , and NpAl_4 , and significantly improves the theoretical prediction accuracy in formation enthalpy for these compounds, reducing the average error to only 9.7%. For the U-Si compounds, the DFT-predicted formation enthalpies of U_3Si_2 , USi , and USi_2 are remarkably higher than experimental values and lie far above the convex hull, incorrectly indicating that these phases are unstable. The predicted average error for all compounds in this system is 28.5%. On the other hand, LCM substantially improves the results: it not only correctly predicted that U_3Si_2 , USi , and USi_2 are stable, but also reduced the average error in the predicted formation enthalpies to only 9.2% compared to the experimental data.

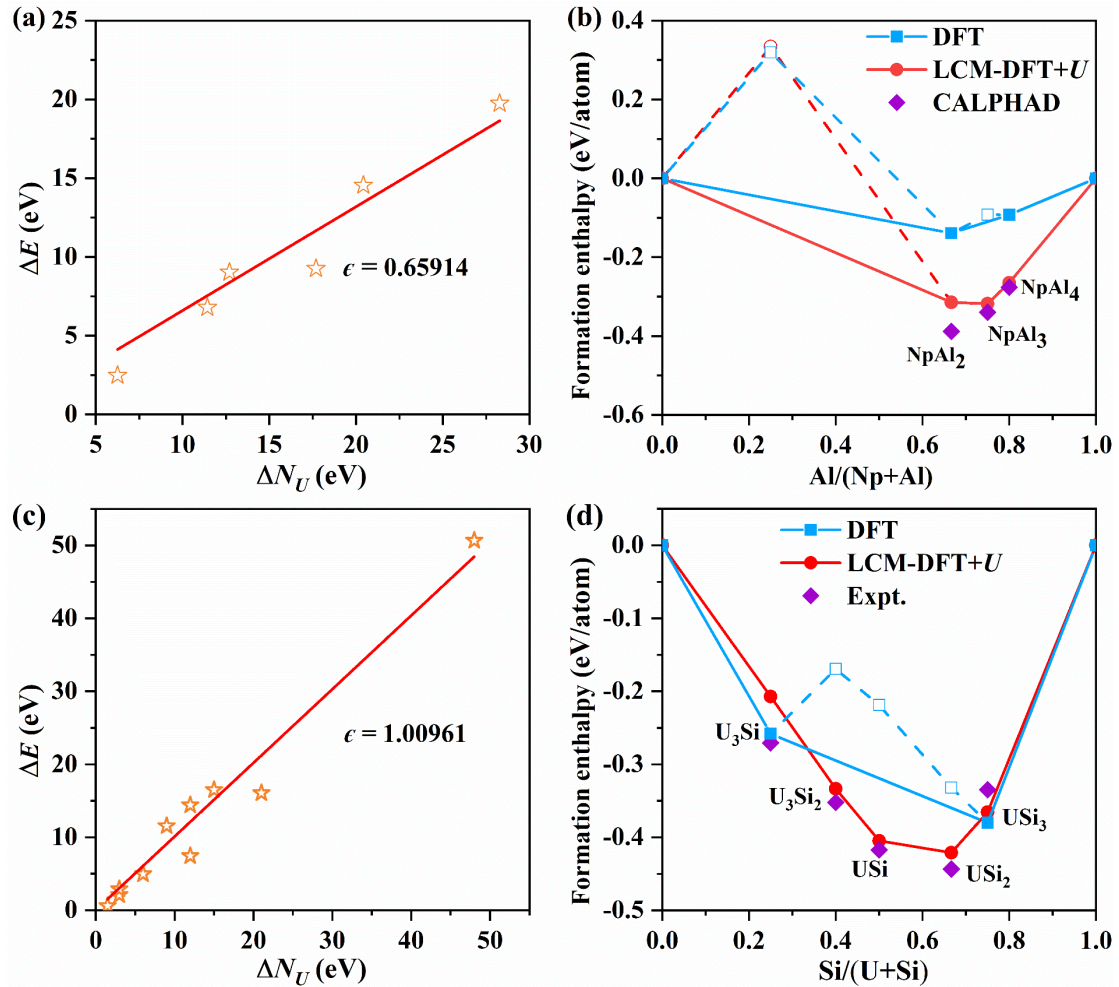


Fig. 5 (color online) Calculated ΔE - ΔN_U relationships and the correction constants for (a) Np-Al and (c) U-Si systems. Thermodynamic convex hull diagrams of candidate structures at ambient conditions calculated by DFT and LCM-DFT+ U methods: (b) Np-Al system, compared with the CALPHAD data [46]; (d) U-Si system, compared with the experimental data [47].

In the second case, we apply the LCM method to the non-actinide system, including bulk Cu-O system, oxygen adsorption on Cu surface, and a ternary system. For the Cu-O bulk system, the LCM-DFT+ U predicted formation enthalpies of CuO and CuO₂ compounds show great improvement over those obtained from pure DFT calculations (Table 2), with the LCM method yielding an average error of 8.4%—substantially lower than the 26.7% error of DFT. Beyond the bulk system, we also employ this method to investigate the adsorption energy of oxygen atom on the Cu(111) surface. Specifically, for an oxygen atom adsorbed at the fcc site on a clean Cu(111) (2×2 supercell) surface, the LCM-DFT+ U calculated adsorption formation enthalpy is

-4.901 eV. This value is slightly closer to the experimental value of -4.467 eV than the DFT result (-5.032 eV), corresponding to an error of 9.7% and 12.7%, respectively. Finally, we apply the LCM method to the ternary MnSnAu system, with the Hubbard term acts on the Mn atoms, for which the LCM also demonstrates excellent performance. The result is that the LCM-predicted formation enthalpy is -0.521 eV/atom, deviating by only 3.8% from the experimental value (-0.502 eV/atom). In contrast, the pure DFT gives a value of -0.053 eV/atom, showing a significantly larger error of 89.4% than LCM.

These additional case studies further demonstrate the power and the general applicability of LCM method, revealing that it can be extended beyond uranium-based binary alloys to include other strongly correlated systems, whether binary or ternary, even surface adsorption.

Table 2. Comparison of calculated formation enthalpies (in eV/O for Cu(111)-O, in eV/atom for other compounds) for different systems at zero pressure using pure DFT (GGA-PBE) and LCM-DFT+*U* methods, together with the corresponding reference data. The reference data for the Np-Al system are taken from the CALPHAD data [46], while those for the other compounds are experimental values in Refs. [24, 47-49].

Compound	DFT	LCM-DFT+ <i>U</i>	Reference data	Error (%)	
				DFT	LCM
NpAl ₂	-0.139	-0.315	-0.388	64.2	18.8
NpAl ₃	-0.092	-0.318	-0.340	72.9	6.5
NpAl ₄	-0.093	-0.265	-0.277	66.4	4.3
U ₃ Si	-0.258	-0.207	-0.271	4.8	23.6
U ₃ Si ₂	-0.170	-0.333	-0.352	51.7	5.4
USi	-0.219	-0.405	-0.417	47.5	2.9
USi ₂	-0.332	-0.421	-0.443	25.1	5.0
USi ₃	-0.380	-0.366	-0.335	13.4	9.3
CuO	-0.938	-0.832	-0.820	14.4	1.5
CuO ₂	-0.806	-0.669	-0.580	39.0	15.3
Cu(111)-O	-5.032	-4.901	-4.467	12.7	9.7
MnSnAu	-0.053	-0.521	-0.502	89.4	3.8

V. Conclusion

A general LCM that is fully *ab initio* to correct the energy (as well as the pressure and enthalpy) of DFT+ X methods introduced by the Hubbard model was proposed, which effectively removed the unphysical dependence of the calculated energetics on the model parameters without requiring any experimental data as input. The validation and accuracy of this method were demonstrated using the framework of DFT+ U for important nuclear materials of U-Ga, U-Al, and U-In systems under ambient conditions. Correct phase stability and lattice structures were obtained. The accuracy in the calculated formation enthalpy of stable phases has been significantly improved from the totally unphysical results of plain DFT+ U to within 6% of the experimental values using the LCM. This perfect reproduction of the experimental formation enthalpy and phase stability of the strongly correlated alloys with a fully first-principles approach is very impressive, and is the first time to the best of our knowledge.

A key feature of the LCM is that it requires no experimental input, which greatly expands the scope for investigating the phase stability and phase diagrams of strongly correlated materials under extreme conditions. In such regimes, DFT+ X methods and accurate first-principles formation enthalpies are essential, while experimental energetic data are often unavailable. To illustrate this capability, the LCM of DFT+ U was applied to high-pressure phases of U-Ga, U-Al, and U-In systems up to 200 GPa. Three new phases were discovered at high pressures: (i) $P6/mmm$ phases of U_2Ga , U_2Al , and U_2In ; (ii) $P-62m$ phases of U_2Ga_3 and U_2Al_3 ; and (iii) $P6/mmm$ phases of UGa_3 and UIn_3 , respectively. Our results indicate that under high pressure, not only the crystal

structures but also the compositions of all known low-pressure intermetallic phases of U-Ga (UGa_3 and UGa_2), U-Al (UAl_2 , UAl_3 , UAl_4), and U-In (UIn_3), lose their stability and decompose. In contrast, new stoichiometries, including U_2Ga_3/U_2Al_3 and $U_2Ga/U_2Al/U_2In$, emerge and become stable. These insights unveiled a completely new physical picture about the uranium based binary alloys with main group elements, and demonstrated the power of the LCM. Furthermore, the broad applicability of LCM has been validated across a range of diverse systems, including binary systems such as Np-Al, U-Si, and Cu-O, as well as in more complex cases such as oxygen adsorption on the Cu(111) surface and the ternary MnSnAu compound. Since applying LCM with other DFT+ X methods is similar to DFT+ U , and is rather straightforward, progress along this line will open a new avenue for accurate description of strongly correlated systems, and will accelerate the discovery of novel correlated materials.

Method and Computational details

Variable-composition structure searches for U-M (M=Ga, Al, In) systems were carried out at five different pressures of 0, 50, 100, 150 and 200 GPa to generate candidate structures, using the evolutionary algorithm as implemented in USPEX package [50]. The unit cell contains up to 24 atoms. The first generation includes 100 random structures and for the remaining generations, each contains 60 structures. A total of 60 generations were generated for every search. The best ten candidate structures for each composition with the lowest enthalpy were then re-optimized with higher computational accuracy to find the most stable structure. Structural relaxation and total energy calculations were performed using DFT [1, 2] as implemented in the Vienna Ab initio Simulation Package (VASP) [51, 52]. The exchange-correlation functional is described by the Perdew-Burke-Ernzerhof (PBE) [53] parameterization of the GGA. The atomic coordinates and lattice vectors were fully optimized until the

Hellmann–Feynman forces acting on each atom were less than 10^{-3} eV/Å and the convergence of the total energy was better than 10^{-7} eV between two successive ionic steps. The cut-off energy of 550 eV for the plane-wave basis set and the Monkhorst-Pack [54] k-point meshes with a grid spacing of $2\pi \times 0.02$ Å⁻¹ were used to ensure that the energy of each structure is converged to 1 meV per atom or better for all calculations. In order to ensure the dynamic stability of the predicted compounds, the phonon dispersion curves were checked by using the small-displacement method as implemented in MyPhon [55].

For systems containing *d* or *f* electrons that exhibit strong electronic correlations, DFT+*U* approach was employed to deal with the on-site coulomb interactions between the *f* electrons of uranium atoms in U-M (M=Al, Ga, In) compounds. Specifically, we used the simplified DFT+*U* method proposed by Dudarev et al. [11] with only a single effective *U* parameter. Linear response method proposed by Cococcioni et al. [56] was used to determine the effective Hubbard *U* value for all U-M compounds through both self-consistent and non-self-consistent calculations within the framework of the PBE, thus renders our DFT+*U* as fully *ab initio*. The consequence is that the Hubbard *U* parameter might be different for different U-M compounds at different pressure, and LCM provides the theoretical basis to handle this variation. Spin polarization was taken into account in different magnetic ordering, including antiferromagnetic (AFM), ferromagnetic (FM), and non-magnetic (NM) ordering. For U-In system, we also considered paramagnetic (PM) ordering. The possible metastable electronic states that is notorious in DFT+*U* calculations were eliminated by using QA method [57]. It should be pointed out that in order to reduce the computational demanding for DFT+*U* calculations, the initial candidate structures were generated by using USPEX with PBE functional. These structures were then screened by structure relaxations with DFT+*U* and the formation enthalpies calculated by plain DFT+*U* or LCM for DFT+*U*, respectively. The obtained structure and energetics, by using pure DFT, plain DFT+*U*, and LCM for DFT+*U*, were then compared with each other.

The same first-principles calculation methods were applied to the systems of Np-Al, U-Si, Cu-O, MnSnAu, and oxygen adsorption on Cu(111) surface, except for them

we mainly focused on LCM performance on the ambient structures, and did not perform structure search at high pressures.

Acknowledgments

This work was supported by National Key R&D Program of China under Grant No. 2021YFB3802300, the fund of national key laboratory of shock wave and detonation physics under Grant No. 2023JCJQLB05401, the NSAF under Grant Nos. U1730248 and U1830101, the National Natural Science Foundation of China under Grant Nos. 12372370, 12202418, 12074274, the Doctoral Research Fund of Southwest University of Science and Technology (Grant No. 25zx7147). Part of the simulation was performed on resources provided by the center for Comput. Mater. Sci. (CCMS) at Tohoku University, Japan.

Author Contribution

Xiao L. Pan: Calculation, Analysis, Writing, Original draft preparation. Hong X. Song: Analysis, Reviewing and Editing. Y. Sun: Analysis, Reviewing. F. C. Wu: Analysis, Writing. H. Wang: Analysis, Reviewing. Y. Chen: Analysis, Reviewing. Xiang R. Chen: Writing, Reviewing and Editing, Fund. Hua Y. Geng: Idea conceiving, Project design, Theory formulating, Writing, Reviewing and Editing, Fund.

References

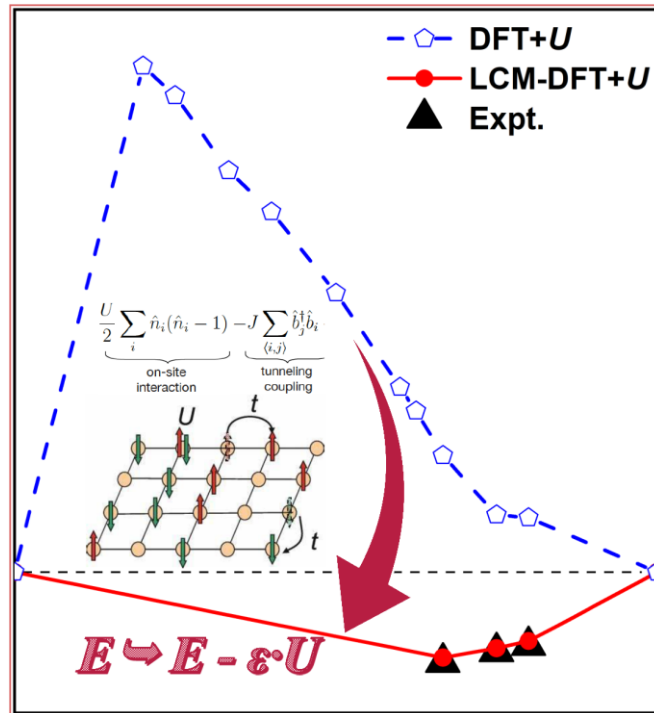
- [1] P. Hohenberg, W. Kohn, Inhomogeneous electron gas, *Phys. Rev.*, **136** (1964) B864-B871.
- [2] W. Kohn, L. J. Sham, Self-consistent equations including exchange and correlation effects, *Phys. Rev.*, **140** (1965) A1133-A1138.
- [3] M. Aydinol, A. Kohan, G. Ceder, K. Cho, J. Joannopoulos, Ab initio study of lithium intercalation in metal oxides and metal dichalcogenides, *Phys. Rev. B*, **56** (1997) 1354.
- [4] N. Skorodumova, S. Simak, B. I. Lundqvist, I. Abrikosov, B. Johansson, Quantum origin of the oxygen storage capability of ceria, *Phys. Rev. Lett.*, **89** (2002) 166601.
- [5] T. Ziegler, J. Autschbach, Theoretical methods of potential use for studies of inorganic reaction mechanisms, *Chem. Rev.*, **105** (2005) 2695-2722.
- [6] K. Kang, Y. S. Meng, J. Breger, C. P. Grey, G. Ceder, Electrodes with high power and high capacity for rechargeable lithium batteries, *Science*, **311** (2006) 977-980.
- [7] J. P. Perdew, A. Zunger, Self-interaction correction to density-functional approximations for many-electron systems, *Phys. Rev. B*, **23** (1981) 5048.
- [8] J. P. Perdew, K. Burke, M. Ernzerhof, Generalized gradient approximation made simple, *Phys.*

- Rev. Lett., **77** (1996) 3865.
- [9] J. Sun, A. Ruzsinszky, J. P. Perdew, Strongly Constrained and Appropriately Normed Semilocal Density Functional, Phys. Rev. Lett., **115** (2015) 036402.
- [10] S. Hüfner, Electronic structure of NiO and related 3d-transition-metal compounds, Adv. Phys., **43** (1994) 183-356.
- [11] S. L. Dudarev, G. A. Botton, S. Y. Savrasov, C. J. Humphreys, A. P. Sutton, Electron-energy-loss spectra and the structural stability of nickel oxide: An LSDA+ U study, Phys. Rev. B, **57** (1998) 1505.
- [12] H. Y. Geng, Y. Chen, Y. Kaneta, M. Kinoshita, Structural behavior of uranium dioxide under pressure by LSDA+ U calculations, Phys. Rev. B, **75** (2007) 054111.
- [13] M. Rahm, N. V. Skorodumova, Phase stability of the rare-earth sesquioxides under pressure, Phys. Rev. B, **80** (2009) 104105.
- [14] Y. X. Wang, H. Y. Geng, Q. Wu, X. R. Chen, Orbital localization error of density functional theory in shear properties of vanadium and niobium, J. Chem. Phys., **152** (2020) 024118.
- [15] V. I. Anisimov, J. Zaanen, O. K. J. P. R. B. Andersen, Band theory and Mott insulators: Hubbard U instead of Stoner I, Phys. Rev. B, **44** (1991) 943.
- [16] X. Y. Deng, L. Wang, X. Dai, Z. Fang, Local density approximation combined with Gutzwiller method for correlated electron systems: Formalism and applications, Phys. Rev. B, **79** (2009) 075114.
- [17] K. M. Ho, J. Schmalian, C. Z. Wang, Gutzwiller density functional theory for correlated electron systems, Phys. Rev. B, **77** (2008) 073101.
- [18] A. Lichtenstein, M. Katsnelson, Ab initio calculations of quasiparticle band structure in correlated systems: LDA++ approach, Phys. Rev. B, **57** (1998) 6884.
- [19] G. Kotliar, S. Y. Savrasov, K. Haule, V. S. Oudovenko, O. Parcollet, C. Marianetti, Electronic structure calculations with dynamical mean-field theory, Rev. Mod. Phys., **78** (2006) 865-951.
- [20] H. J. Kulik, N. Marzari, Accurate potential energy surfaces with a DFT+U(R) approach, J. Chem. Phys., **135** (2011) 194105.
- [21] H. Y. Geng, Y. Chen, Y. Kaneta, M. Iwasawa, T. Ohnuma, M. Kinoshita, Point defects and clustering in uranium dioxide by LSDA+U calculations, Phys. Rev. B, **77** (2008) 104120.
- [22] A. Jain, G. Hautier, S. P. Ong, C. J. Moore, C. C. Fischer, K. A. Persson, G. Ceder, Formation enthalpies by mixing GGA and GGA+U calculations, Phys. Rev. B, **84** (2011) 045115.
- [23] S. Lany, Semiconductor thermochemistry in density functional calculations, Phys. Rev. B, **78** (2008) 245207.
- [24] V. Stevanović, S. Lany, X. Zhang, A. Zunger, Correcting density functional theory for accurate predictions of compound enthalpies of formation: Fitted elemental-phase reference energies, Phys. Rev. B, **85** (2012) 115104.
- [25] M. Aykol, C. Wolverton, Local environment dependent GGA+U method for accurate thermochemistry of transition metal compounds, Phys. Rev. B, **90** (2014) 115105.
- [26] Y. Yu, M. Aykol, C. Wolverton, Reaction thermochemistry of metal sulfides with GGA and GGA+U calculations, Phys. Rev. B, **92** (2015) 195118.
- [27] A. Patra, H. Peng, J. Sun, J. P. Perdew, Rethinking CO adsorption on transition-metal surfaces: Effect of density-driven self-interaction errors, Phys. Rev. B, **100** (2019) 035442.
- [28] Y. X. Wang, Q. Wu, X. R. Chen, H. Y. Geng, Stability of rhombohedral phases in vanadium at high-pressure and high-temperature: first-principles investigations, Sci. Rep., **6** (2016) 32419.

- [29] C. B. Alcock, J. B. Cornish, P. Grieveson, Knudsen effusion studies of compounds of uranium and thorium with elements of groups IIIb and IVb, In *Thermodynamics. Vol. I. Proceedings of the Symposium on Thermodynamics with Emphasis on Nuclear Materials and Atomic Transport in Solids*, 1966.
- [30] B. Prabhakara Reddy, R. Babu, K. Nagarajan, P. R. Vasudeva Rao, Enthalpies of formation of UGa₂ and UGa₃ by calorimetry, *J. Alloys Compd.*, **271** (1998) 395-399.
- [31] M. I. Ivanov, V. A. Tumbakov, N. S. Podolskaya, Heats of formation of UAl sub 2, UAl sub 3, and UAl sub 4, *Atom. Energy*, **5** (1958) 166.
- [32] R. E. Rundle, A. S. Wilson, The structures of some metal compounds of uranium, *Acta Crystallogr.*, **2** (1949) 148-150.
- [33] S. Steeb, G. Petzow, Strukturelle Veränderungen der Laves-Phasen ZrAl₂ und UAl₂ durch Uran-bzw. Zirkonzusätze, *Naturwissenschaften*, **48** (1961) 450-451.
- [34] P. C. Sahu, N. C. Shekar, N. Subramanian, M. Yousuf, K. G. Rajan, Crystal structure of UAl₂ above 10 GPa at 300 K, *J. Alloys Compd.*, **223** (1995) 49-52.
- [35] O. Tougait, H. Noël, Stoichiometry of UAl₄, *Intermetallics*, **12** (2004) 219-223.
- [36] D. Dayan, G. Kimmel, M. P. Dariel, Shear-like transformation in β -stabilized U-1.5 at% Ga alloy; structure of the intermetallic compound U₃Ga₅, *J. Nucl. Mater.*, **135** (1985) 40-45.
- [37] C. Moussa, A. Berche, J. Barbosa, M. Pasturel, B. Stepnik, O. Tougait, Experimental investigation of the phase equilibria and thermodynamic assessment in the U-Ga and U-Al-Ga systems, *J. Nucl. Mater.*, **499** (2018) 361-371.
- [38] K. H. J. Buschow, Phase relationships and magnetic properties of uranium-gallium compounds, *J. Less Common Met.*, **31** (1973) 165-168.
- [39] A. C. Lawson, A. Williams, J. L. Smith, P. A. Seeger, J. A. Goldstone, J. A. O'rourke, Z. Fisk, Magnetic neutron diffraction study of UGa₃ and UGa₂, *J. Magn. Magn. Mater.*, **50** (1985) 83-87.
- [40] X. L. Pan, H. Wang, L. L. Zhang, Y. F. Wang, X. R. Chen, H. Y. Geng, Y. Chen, Prediction of novel final phases in aged uranium-niobium alloys, *J. Nucl. Mater.*, **579** (2023) 154394.
- [41] X. L. Pan, H. X. Song, H. Wang, F. C. Wu, Y. C. Gan, X. R. Chen, Y. Chen, H. Y. Geng, Prediction of novel ordered phases in U-X (X= Zr, Sc, Ti, V, Cr, Y, Nb, Mo, Hf, Ta, W) binary alloys under high pressure, *Acta Mater.*, **263** (2024) 119489.
- [42] A. V. Andreev, K. P. Belov, A. V. Deryagin, Z. A. Kazei, R. Z. Levitin, A. Meňovský, Y. F. Popov, V. I. Silant'ev, Crystal structure, and magnetic and magnetoelastic properties of UGa₂, *Sov. Phys. JETP*, **48** (1978) 1187.
- [43] M. Usuda, J.-i. Igarashi, A. Kodama, Magnetic resonant x-ray scattering at the Ga K edge in UGa₃: A band theoretical approach, *Phys. Rev. B*, **69** (2004) 224402.
- [44] P. Dervenagas, D. Kaczorowski, F. Bourdarot, P. Burlet, A. Czopnik, G. H. Lander, Neutron diffraction on a UGa₃ single crystal, *Physica B*, **269** (1999) 368-372.
- [45] J. M. Lawrence, M. L. Den Boer, R. D. Parks, J. L. Smith, X-ray absorption spectra in rare-earth and uranium intermetallics: localized versus itinerant final states, *Phys. Rev. B*, **29** (1984) 568.
- [46] D. Sedmidubský, R. J. M. Konings, P. Souček, Ab-initio calculations and phase diagram assessments of An–Al systems (An= U, Np, Pu), *J. Nucl. Mater.*, **397** (2010) 1-7.
- [47] A. Berche, C. Rado, O. Rapaud, C. Guéneau, J. Rogez, Thermodynamic study of the U–Si system, *J. Nucl. Mater.*, **389** (2009) 101-107.
- [48] E. Shustorovich, A. T. Bell, Oxygen-assisted cleavage of O H, N H, and C H bonds on transition metal surfaces: bond-order-conservation-Morse-potential analysis, *Surf. Sci.*, **268** (1992) 397-405.

- [49] G. Kim, S. V. Meschel, P. Nash, W. Chen, Experimental formation enthalpies for intermetallic phases and other inorganic compounds, *4* (2017) 1-11.
- [50] A. R. Oganov, C. W. Glass, Crystal structure prediction using ab initio evolutionary techniques: Principles and applications, *J. Chem. Phys.*, **124** (2006) 244704.
- [51] G. Kresse, J. Hafner, Ab initio molecular dynamics for liquid metals, *Phys. Rev. B*, **47** (1993) 558-561.
- [52] G. Kresse, J. Furthmuller, Efficiency of ab-initio total energy calculations for metals and semiconductors using a plane-wave basis set, *Comput. Mater. Sci.*, **6** (1996) 15-50.
- [53] J. P. Perdew, K. Burke, M. Ernzerhof, Generalized gradient approximation made simple, *Phys. Rev. Lett.*, **77** (1996) 3865.
- [54] H. J. Monkhorst, J. D. Pack, Special points for Brillouin-zone integrations, *Phys. Rev. B*, **13** (1976) 5188-5192.
- [55] H. Y. Geng, Full temperature-dependent potential and anharmonicity in metallic hydrogen: Colossal NQE and the consequences, *J. Phys. Chem. C*, **126** (2022) 19355-19366.
- [56] M. Cococcioni, S. de Gironcoli, Linear response approach to the calculation of the effective interaction parameters in the LDA+U method, *Phys. Rev. B*, **71** (2005) 035105.
- [57] H. Y. Geng, Y. Chen, Y. Kaneta, M. Kinoshita, Q. Wu, Interplay of defect cluster and the stability of xenon in uranium dioxide from density functional calculations, *Phys. Rev. B*, **82** (2010) 094106.

TOC



Hubbard model is pivotal to describe strongly correlated materials. But when incorporated with DFT to form DFT+ U , or generally DFT+ X method, its energy becomes dependent on the model parameters and not well-defined. This notorious problem leads to unphysical formation energy. Linear correction method proposed here successfully eliminate the ambiguity in the energetics of DFT+ X , and gives rise to the accurate formation enthalpy that is in excellent agreement with experimental data for the first time. This progress allows self-consistently varying of the model parameters, thus unprecedentedly makes DFT+ U a purely ab initio method.

Supplementary Material for “General linear correction method for DFT+*X* energy: application to U-M (M=Al, Ga, In) alloys under high pressure”

Xiao L. Pan^{1,2,3}, Hong X. Song¹, Y. Sun¹, F. C. Wu^{1*}, H. Wang¹, Y. F. Wang¹, Y. Chen⁵, Xiang R. Chen^{2*}, Hua Y. Geng^{1,4*}

¹ National Key Laboratory of Shock Wave and Detonation Physics, Institute of Fluid Physics, China Academy of Engineering Physics, Mianyang, Sichuan 621900, P. R. China;

² College of Physics, Sichuan University, Chengdu 610065, P. R. China;

³ Extreme Condition Material Properties Science and Technology center, School of Mathematics and Physics, Southwest University of Science and Technology, Mianyang, 621010, P. R. China;

⁴ HEDPS, Center for Applied Physics and Technology, and College of Engineering, Peking University, Beijing 100871, P. R. China;

⁵ Fracture and Reliability Research Institute, School of Engineering, Tohoku University, Sendai 980-8579, Japan.

SI. Supplementary computational details

In order to determine the dynamic stability of the predicted intermetallic compounds, the phonon dispersion curves were calculated using the small-displacement method implemented in MyPhon code [1]. A $2 \times 2 \times 4$ supercell for *P6/mmm*-U₂M (48 atoms), $2 \times 1 \times 2$ supercell for U₃M (64 atoms), $2 \times 2 \times 1$ supercell for *Immm*-U₄M (40 atoms), $2 \times 2 \times 1$ supercell for *Pmma*-U₃M₂ (40 atoms), $2 \times 2 \times 1$ supercell for *P-62m*-U₂M₃ (40 atoms), $2 \times 2 \times 2$ supercell for UM₃ (32 atoms), $2 \times 2 \times 1$ supercell for *P6₃/mmc*-UAl₃ (96 atoms), and $2 \times 2 \times 1$ supercell for *Imma*-UAl₄ (80 atoms) were employed in the calculations of phonon spectra.

The linear response method proposed by Cococcioni *et al.* [2] was used to theoretically and self-consistently determine the Hubbard *U* value for all U-M compounds at each pressure through both self-consistent and non-self-consistent

* Corresponding authors. E-mail: s102genghy@caep.cn; xrchen@scu.edu.cn; fcwu2011@mail.ustc.edu.cn

calculations within the framework of PBE in VASP. This renders our DFT+ U as fully *ab initio* (in the sense that does not require any experimental or empirical input), and the specific U value varies with structure, composition and pressure. In the linear response method, by applying an additional spherical potential to a single uranium atom in U-M compounds, the f -orbital charge density of the uranium atom is redistributed. Thus, both self-consistent and non-self-consistent response functions can be obtained by following equations:

$$\chi = \left(\frac{\partial N^{\text{scf}}}{\partial V} \right), \quad \chi_0 = \left(\frac{\partial N^{\text{nscf}}}{\partial V} \right) \quad (1)$$

where V represents the applied additional spherical potential, N^{scf} and N^{nscf} represent the f -electrons number of uranium atom obtained via self-consistent and non-self-consistent calculations under the additional spherical potential, respectively. With the non-self-consistent and the self-consistent response functions, the self-consistent value of U parameter for the DFT+ U treatment of the uranium f -electrons in U-M compounds is obtained by the following equation:

$$U = \chi^{-1} - \chi_0^{-1} = \left(\frac{\partial N^{\text{scf}}}{\partial V} \right)^{-1} - \left(\frac{\partial N^{\text{nscf}}}{\partial V} \right)^{-1} \quad (2)$$

In order to get accurate result, six additional potentials (-0.1, -0.05, -0.025, 0.025, 0.05, and 0.1 eV) were used for the self-consistent and non-self-consistent calculations. The corresponding response function was then obtained by linearly fitting the f -electrons number of uranium atom as a function of the additional potential V .

In the DFT+ U calculations for the Np - Al system, the Hubbard U parameters for each compound were determined using the linear response method. The resulting U values are 2.618 eV for Np₃Al, 2.997 eV for NpAl₂, 3.140 eV for NpAl₃, and 3.135 eV for NpAl₄. For the U - Si, Cu - O, and MnSnAu systems, a single Hubbard U value was employed for all compounds within each system for brevity, namely 1.5 eV for U - Si, 4.0 eV for Cu - O, and 4.0 eV for MnSnAu. In our calculations, the O₂ energy is corrected following Wang et al. [3], which removes oxygen-related GGA errors and enables a reliable assessment of the Hubbard U correction applied to the Cu d orbitals.

SII. Supplementary figures

A. The Hubbard U parameters used in DFT+ U calculations

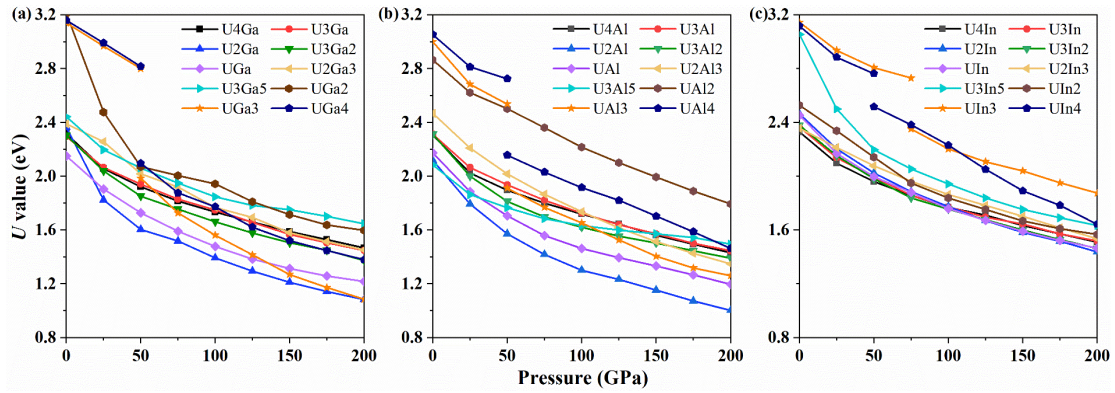


Fig. S1 (color online) Variation of the calculated Hubbard U parameter as a function of pressure for all U-M compounds. They are used in subsequent DFT+ U calculations. (a) U-Ga system; (b) U-Al system; (c) U-In system. Note that these U parameters are obtained via the linear response method. For UM_3 and UM_4 ($M=Ga, Al, In$) compositions, the jump in U indicates that the structure is changed at that pressure.

B. Comparison of formation enthalpies calculated by LCM-DFT+ U and plain DFT+ U methods

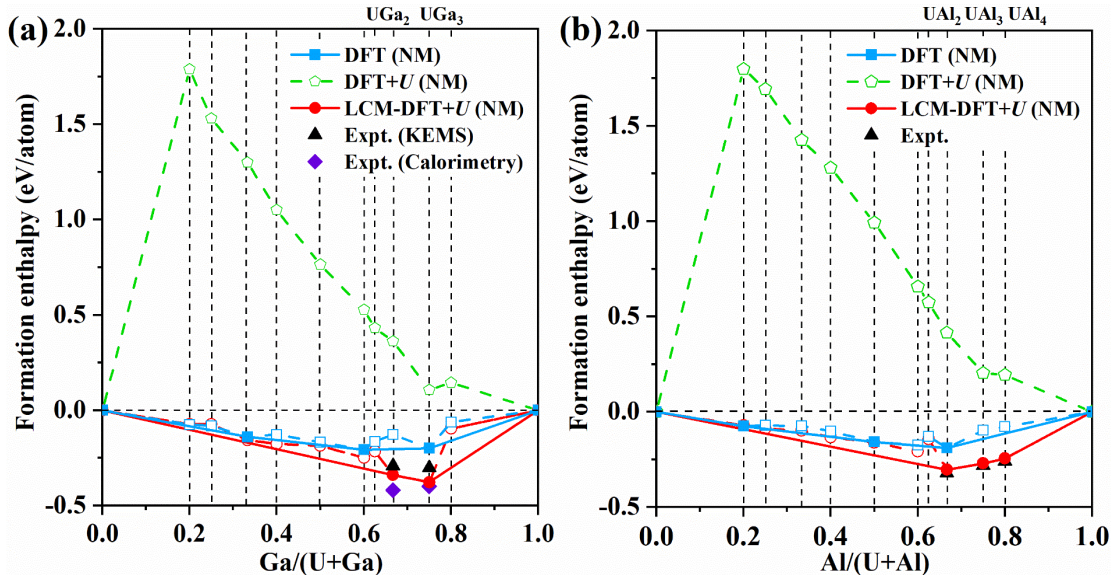


Fig. S2 (color online) Comparison of the thermodynamic convex hull diagrams of candidate structures at ambient conditions calculated by pure DFT, plain DFT+ U , and LCM-DFT+ U methods: (a) U-Ga system, along with experimental data taken from

Knudsen Effusion Mass Spectrometry (KEMS) [4] and Calorimetry [5] for comparison; (b) U-Al system, along with the experimental data [6]. Dashed-line connections indicate unstable or metastable phases, while solid-line connections indicate stable phases. Here the “plain DFT+ U ” means the formation enthalpy is calculated directly using Eq. (5) of the main text with the energetics of DFT+ U without any correction.

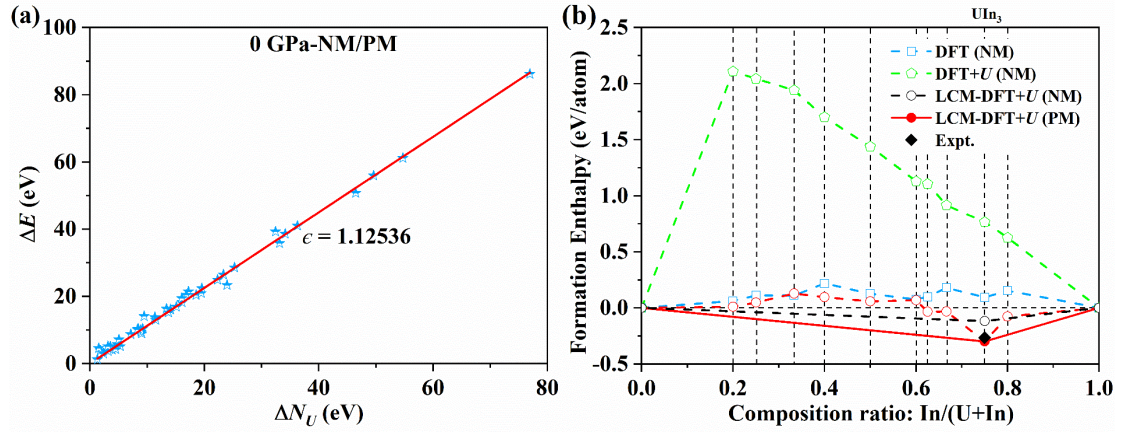


Fig. S3 (color online) (a) The ΔE - ΔN_U relationship for U-In system at ambient conditions, considering paramagnetic ordering for $Pm-3m$ - UIn_3 and nonmagnetic ordering for other compositions. For the paramagnetic phase calculation of $Pm-3m$ - UIn_3 , we used a $2 \times 2 \times 2$ supercell (32 atoms), fixing the magnetic moment of each atom at $2.75 \mu_B$ but with random directions, while ensuring the total magnetic moment of the system remains zero. Eight sets of random magnetic moment directions were considered, and the averaged energy of these configurations was used to calculate the formation enthalpy of the $Pm-3m$ - UIn_3 in paramagnetic state. (b) Comparison of the thermodynamic convex hull diagrams of candidate structures at ambient conditions calculated by pure DFT, plain DFT+ U , and LCM-DFT+ U methods with the experimental data [6], respectively. Here the NM and PM denote nonmagnetic and paramagnetic ordering, respectively.

C. The ΔE - ΔN_U relationship of U-M compounds at different pressures

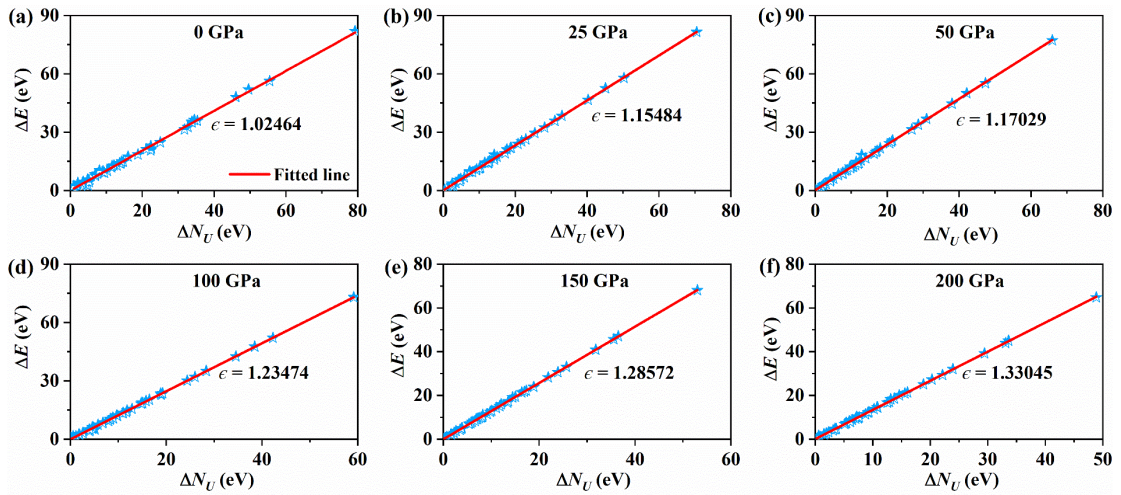


Fig. S4 The ΔE - ΔN_U relationship for U-Ga system at 0 K and at pressures of 0, 25, 50, 100, 150, and 200 GPa, respectively. The magnetic ordering (NM, FM or AFM) has been taken into account.

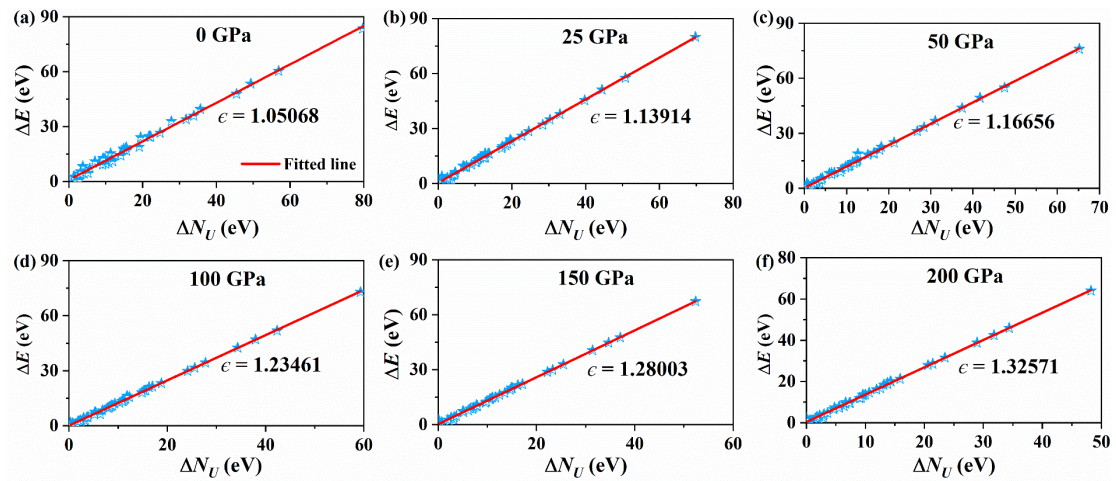


Fig. S5 The ΔE - ΔN_U relationship for U-Al system at 0 K and at pressures of 0, 25, 50, 100, 150, and 200 GPa, respectively. The magnetic ordering (NM, FM or AFM) has been taken into account.

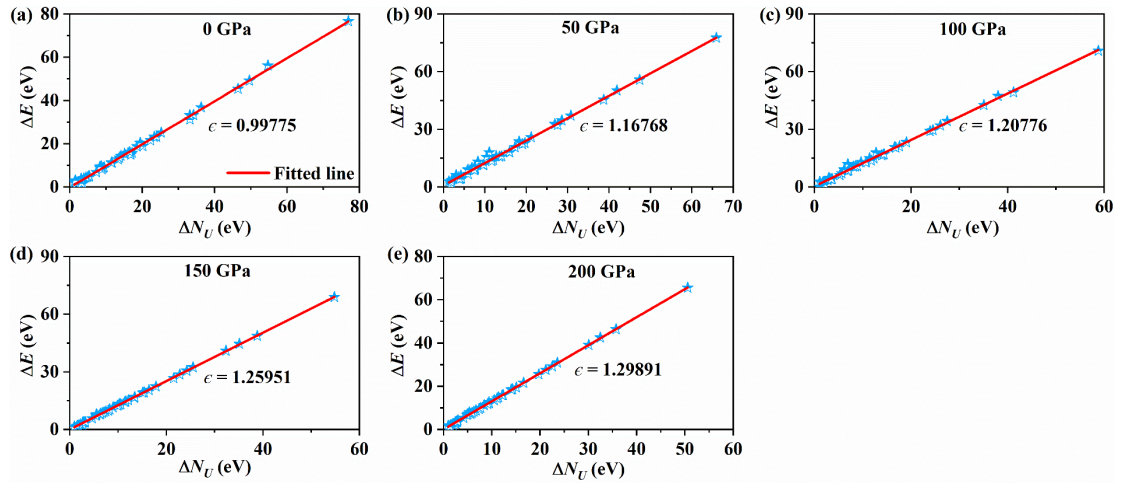


Fig. S6 The ΔE - ΔN_U relationship for U-In system at 0 K and at pressures of 0, 50, 100, 150, and 200 GPa, respectively. The magnetic ordering (NM, FM or AFM) has been taken into account.

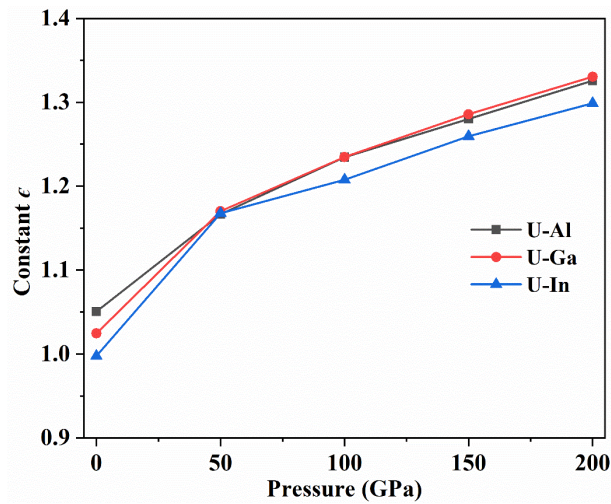


Fig. S7 Variation of the constant ϵ with pressure for U-Al, U-Ga, and U-In systems, as listed in Figs. S4-S6, respectively.

D. Phonon spectra

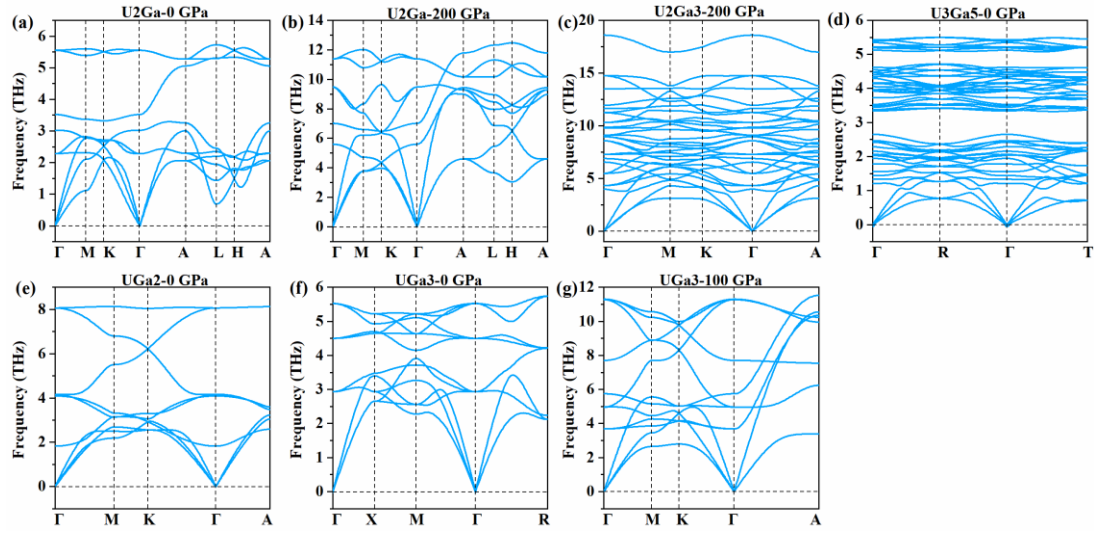


Fig. S8 Calculated phonon spectra for $P6/mmm$ - U_2Ga at (a) 0 GPa and (b) 200 GPa, (c) $P-62m$ - U_2Ga_3 at 200 GPa, (d) $Cmcm$ - U_3Ga_5 at 0 GPa, (e) $P6/mmm$ - UGa_2 at 0 GPa, (f) $Pm-3m$ - UGa_3 at 0 GPa, and (g) $P6/mmm$ - UGa_3 at 100 GPa, respectively.

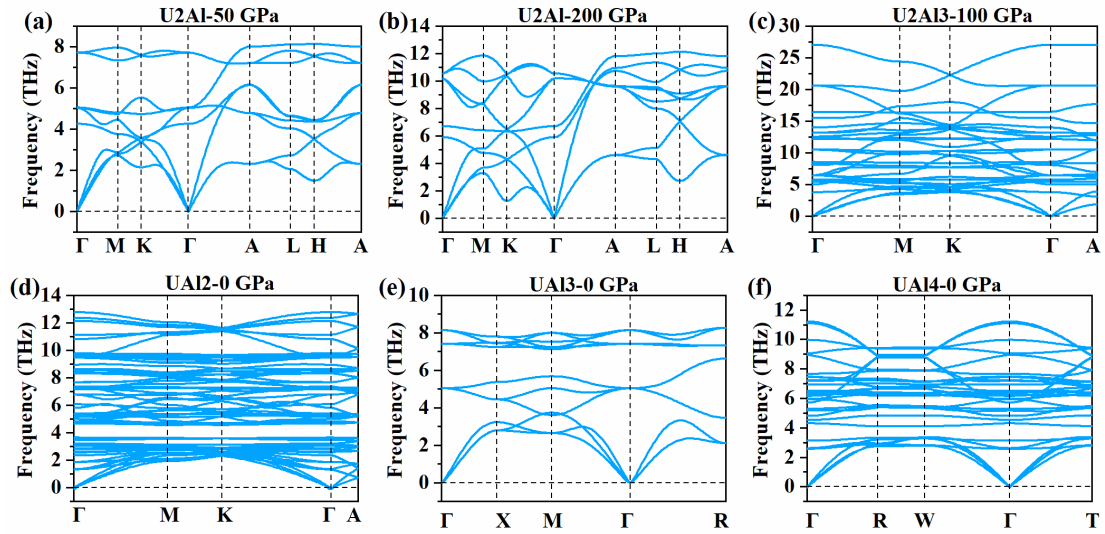


Fig. S9 Calculated phonon spectra for $P6/mmm$ - U_2Al at (a) 50 GPa and (b) 200 GPa, (c) $P-62m$ - U_2Al_3 at 100 GPa, (d) $P6_3/mmc$ - UAl_2 at 0 GPa, (e) $Pm-3m$ - UAl_3 at 0 GPa, and (f) $Imma$ - UAl_4 at 100 GPa, respectively.

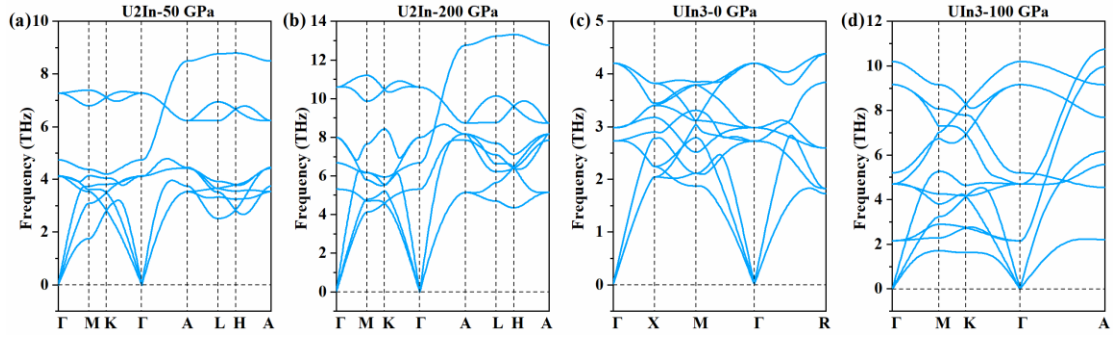


Fig. S10 Calculated phonon spectra for $P6/mmm-U_2In$ at (a) 50 GPa and (b) 200 GPa, (c) $Pm-3m-UIn_3$ at 0 GPa, and (d) $P6/mmm-UIn_3$ at 100 GPa, respectively.

E. Electronic structure and bonding properties

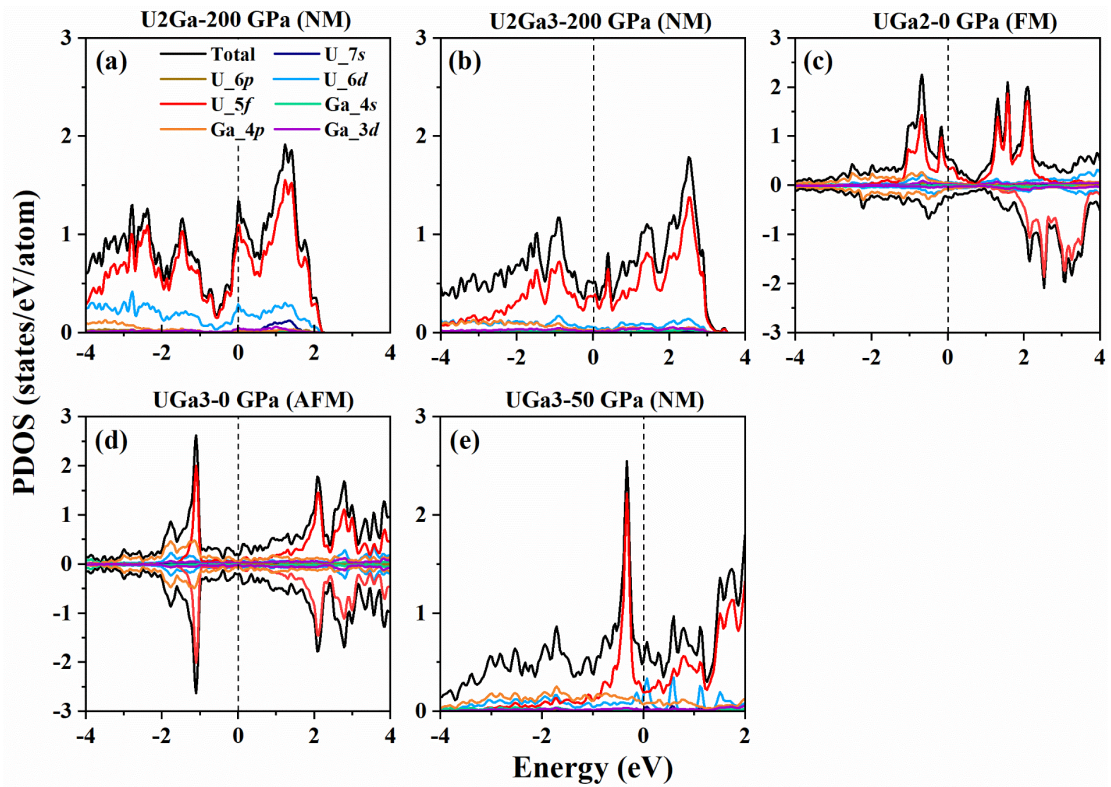


Fig. S11 (color online) Calculated electronic projected density of states (PDOS) for (a) $P6/mmm-U_2Ga$ (NM) at 200 GPa, (b) $P-62m-U_2Ga_3$ (NM) at 200 GPa, (c) $P6/mmm-UGa_2$ (FM) at 0 GPa, (d) $Pm-3m-UGa_3$ (AFM) at 0 GPa, (e) $P6/mmm-UGa_3$ (NM) at 50 GPa, respectively.

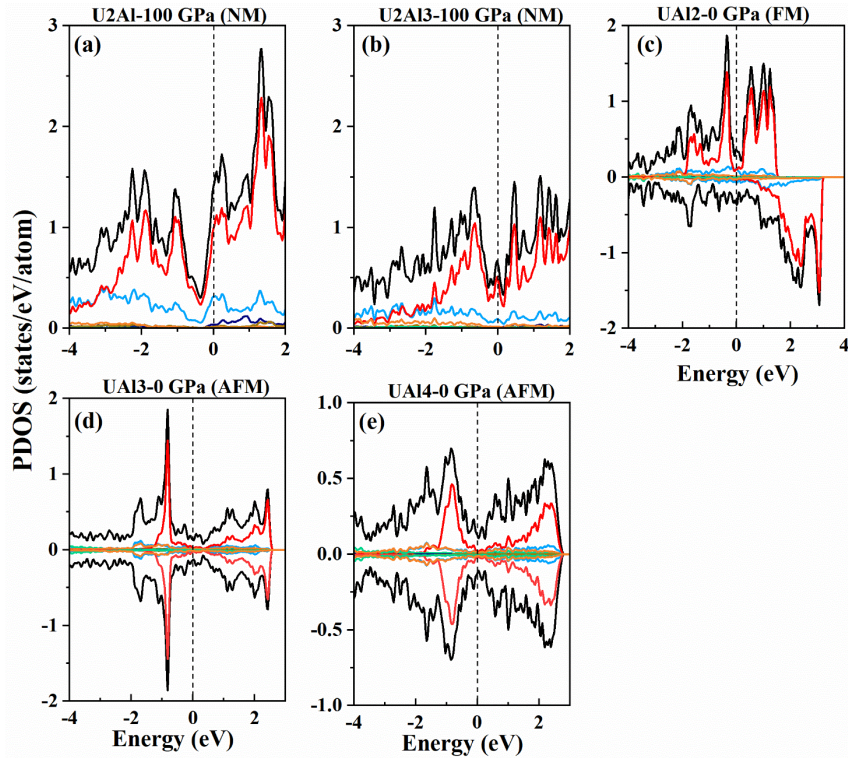


Fig. S12 (color online) Calculated electronic projected density of states (PDOS) for (a) $P6/mmm$ - U_2Al (NM) at 100 GPa, (b) $P-62m$ - U_2Al_3 (NM) at 100 GPa, (c) $P6_3/mmc$ - UAl_2 (FM) at 0 GPa, (d) $Pm-3m$ - UAl_3 (AFM) at 0 GPa, (e) $Imma$ - UAl_4 (AFM) at 0 GPa, respectively.

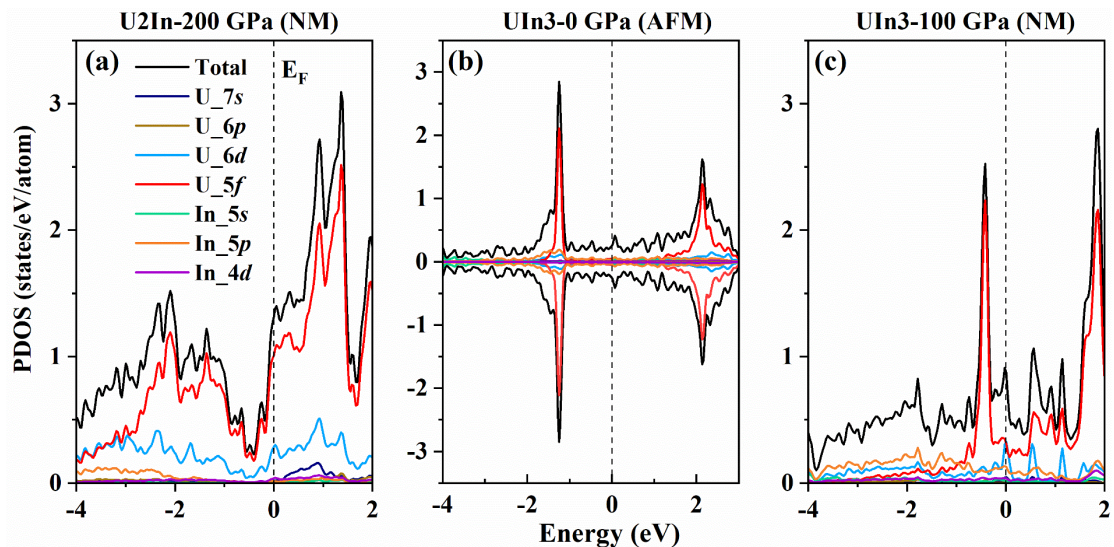


Fig. S13 (color online) Calculated electronic projected density of states (PDOS) for (a) $P6/mmm$ - U_2In (NM) at 200 GPa, (b) $Pm-3m$ - UIn_3 (AFM) at 0 GPa, (c) $P6/mmm$ - UIn_3 (NM) at 100 GPa, respectively.

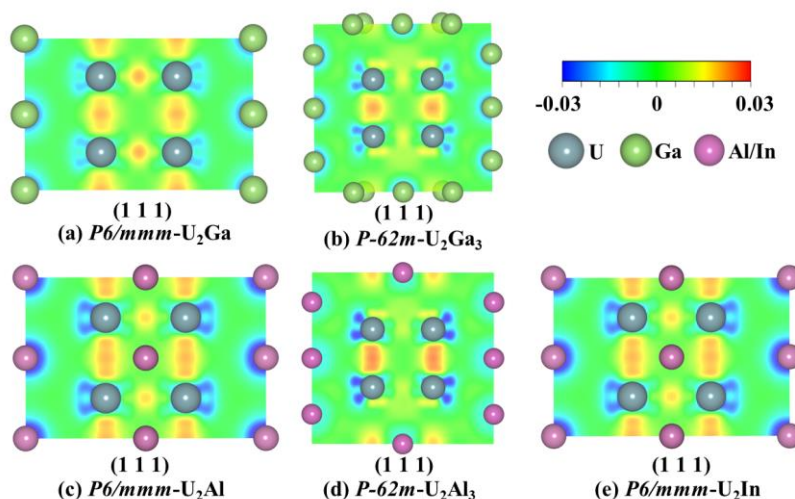


Fig. S14 (color online) Differential charge density for stable ordered phases in U-M (M=Ga, Al, In) systems: (a) $P6/mmm$ - U_2Ga at 150 GPa, (b) $P-62m$ - U_2Ga_3 at 150 GPa; (c) $P6/mmm$ - U_2Al at 100 GPa, (d) $P-62m$ - U_2Al_3 at 100 GPa; (e) $P6/mmm$ - U_2In at 200 GPa, respectively. The blue color indicates the loss of electrons, and yellow indicates the accumulation of charges between neighbouring uranium atoms. The formation of U-U bonds is evident.

F. The ΔE - ΔN_U relationship for other compounds

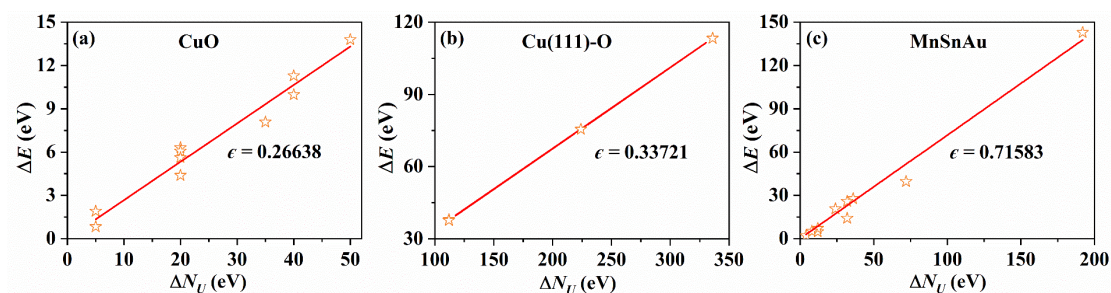


Fig. S15 The ΔE - ΔN_U relationships and the correction constants of the LCM method for the (a) binary bulk Cu-O, (b) oxygen adsorption on Cu(111) surface Cu(111)-O, and (c) ternary MnSnAu systems.

SI. Supplementary table

Table S1. Lattice parameters, atomic coordinates and Wyckoff sites occupation of the newly discovered stable phases $P6/mmm-U_2Ga$, $P-62m-U_2Ga_3$, $P6/mmm-UGa_3$, $P-62m-U_2Al_3$, $P6/mmm-U_2Al$, $P6/mmm-UIn_3$, and $P6/mmm-U_2In$ at the given pressure, respectively.

Phase	Lattice parameters (Å)	Atom	Site	Atomic coordinates
$P6/mmm-U_2Ga$ (150 GPa)	a=b=4.4338 c=2.5644 $\alpha=\beta=90^\circ$ $\gamma=120^\circ$	U	2d	(0.33333, 0.66667, 0.50000)
		Ga	1a	(0.00000, 0.00000, 0.00000)
$P-62m-U_2Ga_3$ (150 GPa)	a=b=4.3376 c=7.0907 $\alpha=\beta=90^\circ$ $\gamma=120^\circ$	U	4h	(0.33333, 0.66667, 0.33021)
		Ga	1b	(0.00000, 0.00000, 0.50000)
			2e	(0.00000, 0.00000, 0.18315)
3f	(0.55872, 0.00000, 0.00000)			
$P6/mmm-UGa_3$ (50 GPa)	a=b=5.11031 c=2.5183 $\alpha=\beta=90^\circ$ $\gamma=120^\circ$	U	1a	(0.00000, 0.00000, 0.00000)
		Ga	1a	(0.50000, 0.50000, 0.50000)
			1a	(0.00000, 0.50000, 0.50000)
1a	(0.50000, 0.00000, 0.50000)			
$P-62m-U_2Al_3$ (100 GPa)	a=b=4.4366 c=7.2464 $\alpha=\beta=90^\circ$ $\gamma=120^\circ$	U	4h	(0.33333, 0.66667, 0.33032)
		Al	3f	(0.50030, 0.00000, 0.00000)
			2e	(0.00000, 0.00000, 0.17293)
1b	(0.00000, 0.00000, 0.50000)			
$P6/mmm-U_2Al$ (100 GPa)	a=b=4.3063 c=2.4901 $\alpha=\beta=90^\circ$ $\gamma=120^\circ$	U	2d	(0.33333, 0.66667, 0.50000)
		Al	1a	(0.00000, 0.00000, 0.00000)
$P6/mmm-UIn_3$ (100 GPa)	a=b=5.2812 c=2.5592 $\alpha=\beta=90^\circ$ $\gamma=120^\circ$	U	1a	(0.00000, 0.00000, 0.00000)
		In	1a	(0.50000, 0.50000, 0.50000)
			1a	(0.00000, 0.50000, 0.50000)
1a	(0.50000, 0.00000, 0.50000)			
$P6/mmm-U_2In$ (200 GPa)	a=b=4.2377 c=2.4499 $\alpha=\beta=90^\circ$ $\gamma=120^\circ$	U	2d	(0.33333, 0.66667, 0.50000)
		In	1a	(0.00000, 0.00000, 0.00000)

Supplementary references

- [1] H. Y. Geng, Full temperature-dependent potential and anharmonicity in metallic hydrogen: Colossal NQE and the consequences, *J. Phys. Chem. C*, **126** (2022) 19355-19366.
- [2] M. Cococcioni, S. de Gironcoli, Linear response approach to the calculation of the effective interaction parameters in the LDA+*U* method, *Phys. Rev. B*, **71** (2005) 035105.
- [3] L. Wang, T. Maxisch, G. Ceder, Oxidation energies of transition metal oxides within the GGA+*U* framework, *Phys. Rev. B*, **73** (2006) 195107.
- [4] C. B. Alcock, J. B. Cornish, P. Grieveson, Knudsen effusion studies of compounds of uranium and thorium with elements of groups IIIb and IVb, In *Thermodynamics. Vol. I. Proceedings of the Symposium on Thermodynamics with Emphasis on Nuclear Materials and Atomic Transport in Solids*, 1966.
- [5] B. Prabhakara Reddy, R. Babu, K. Nagarajan, P. R. Vasudeva Rao, Enthalpies of formation of UGa₂ and UGa₃ by calorimetry, *J. Alloys Compd.*, **271** (1998) 395-399.
- [6] M. I. Ivanov, V. A. Tumbakov, N. S. Podolskaya, Heats of formation of UAl sub 2, UAl sub 3, and UAl sub 4, *Atom. Energy*, **5** (1958) 166.